



miR-210 is overexpressed in late stages of lung cancer and mediates mitochondrial alterations associated with modulation of HIF-1 activity

Bernard Mari, Marie-Pierre Puissegur, Nathalie Mazure, Thomas Bertero, Ludivine Pradelli, Sebastien Grosso, Karine Robbe-Sermesant, Thomas Maurin, Kevin Lebrigand, Bruno Cardinaud, et al.

► To cite this version:

Bernard Mari, Marie-Pierre Puissegur, Nathalie Mazure, Thomas Bertero, Ludivine Pradelli, et al.. miR-210 is overexpressed in late stages of lung cancer and mediates mitochondrial alterations associated with modulation of HIF-1 activity. Cell Death and Differentiation, 2010, 10.1038/cdd.2010.119 . hal-00581855

HAL Id: hal-00581855

<https://hal.science/hal-00581855>

Submitted on 1 Apr 2011

HAL is a multi-disciplinary open access archive for the deposit and dissemination of scientific research documents, whether they are published or not. The documents may come from teaching and research institutions in France or abroad, or from public or private research centers.

L'archive ouverte pluridisciplinaire **HAL**, est destinée au dépôt et à la diffusion de documents scientifiques de niveau recherche, publiés ou non, émanant des établissements d'enseignement et de recherche français ou étrangers, des laboratoires publics ou privés.

miR-210 is overexpressed in late stages of lung cancer and mediates mitochondrial alterations associated with modulation of HIF-1 activity

Marie-Pierre Puisségur^{1,2¶}, Nathalie M. Mazure^{2,3}, Thomas Bertero^{1,2¶}, Ludivine Pradelli^{2,4}, Sébastien Grosso^{1,2}, Karine Robbe-Sermesant^{1,2}, Thomas Maurin^{1,2¶}, Kevin Lebrigand^{1,2}, Bruno Cardinaud^{1,2¶}, Véronique Hofman^{2,4}, Sandra Fourre^{1,2}, Virginie Magnone^{1,2}, Jean Ehrland Ricci^{2,5}, Jacques Pouysségur^{2,3}, Pierre Gounon^{2,6}, Paul Hofman^{2,4}, Pascal Barbry^{1,2§} and Bernard Mari^{1,2§}

(1) CNRS, Institut de Pharmacologie Moléculaire et Cellulaire, UMR6097, F-06560 Sophia Antipolis, France

(2) University of Nice Sophia-Antipolis, Nice, France

(3) CNRS UMR 6543, Centre Antoine Lacassagne, 06189 Nice, France

(4) ERI21/EA 4319, Laboratory of Clinical and Experimental Pathology and Human Biobank Unit, University Hospital Centre of Nice, Nice, France

(5) Inserm, U895, Centre Méditerranéen de Médecine Moléculaire (C3M), Nice, F-06204 Cedex 3, France

(6) Centre Commun de Microscopie Appliquée, Université de Nice-Sophia Antipolis, F-06108 Nice, France

(¶) Present address: MPP: INSERM U563, Centre de Physiopathologie de Toulouse-Purpan, 31300 Toulouse, France ; TB : INSERM U634, 28, Avenue de Valombrose, 06107 NICE, France; TM: Memorial Sloan Kettering Cancer Center Rockefeller Laboratories, New York, NY,

10065, USA ; BC: INSERM U876, ESTBB, Université Bordeaux2, 146 rue Léo Saignat, 33076 Bordeaux, France.

(§) Correspondence to: Pascal Barbry & Bernard Mari, IPMC, CNRS UMR6097, 660, route des lucioles, F06560 Sophia Antipolis, France. Tel: (33) 493 957 793. Fax: (33) 493 957 794. Email: direction@ipmc.cnrs.fr; mari@unice.fr

Running title: MiR-210 targets mitochondrial complex II

Key Words: microRNA, Non-Small Cell Lung Cancer, Electron Transport Chain Complex, hypoxia, apoptosis

Funding source: This work was supported by Association pour la Recherche contre le Cancer (ARC post-doctoral Fellowship to MPP and Grant N°1122 to JER), Cancéropole PACA (PB, PH, BM), INCa (PL0079, PB), European Community (MICROENVIMET, FP7-HEALTH-F2-2008-201279, PB, BM and METOXIA FP7 to NMM and JP), and PHRC Grant 2003 CHU Nice (BM, PB, KL, VH, PH).

ABSTRACT

Following the identification of a set of hypoxia-regulated microRNAs (miRNAs), recent studies have highlighted the importance of miR-210 and of its transcriptional regulation by the transcription factor Hypoxia-Inducible Factor-1 (HIF-1). We report here that miR-210 is overexpressed at late stages of Non-Small Cell Lung Cancer. Expression of miR-210 in lung adenocarcinoma A549 cells caused an alteration of cell viability associated with induction of caspase-3/7 activity. MiR-210 induced a loss of mitochondrial membrane potential and the apparition of an aberrant mitochondrial phenotype. Expression profiling of cells overexpressing miR-210 revealed a specific signature characterized by enrichment for transcripts related to “cell death” and “mitochondrial dysfunction”, including several subunits of the Electron Transport Chain (ETC) complexes I and II. The transcript coding for one of these ETC components, SDHD, a subunit of Succinate Dehydrogenase (SDH) was validated as a *bona fide* miR-210 target, *SDHD* knockdown mimicking miR-210-mediated mitochondrial alterations. Finally, miR-210-dependent targeting of SDHD was able to activate HIF-1, in line with previous studies linking loss-of-function SDH mutations to HIF-1 activation. MiR-210 can thus regulate mitochondrial function by targeting key ETC components genes with important consequences on cell metabolism, survival and modulation of HIF-1 activity. These observations help explain contradictory data about miR-210 expression and its putative function in solid tumors.

Introduction

Lung cancer is the leading cause of cancer deaths in Western countries ¹. Despite therapeutic improvements, prognosis of lung cancer is poor. Recent technical developments have focused on identifying specific gene expression signatures associated with tumor staging and patient prognosis to improve prognosis and therapy ². Interestingly, microRNAs (miRNAs) tumor expression appears to be more accurate in determining the classification of cancer subtypes than classical mRNA expression profiles ³. Analysis of the “miRNome” from human lung tumor samples identified a miRNA signature composed of a large portion of down-regulated miRNAs, including let-7, miR-16 and miR-125 and a set of overexpressed miRNAs, such as miR-21, miR-191, miR-155 and members of the cluster miR-17-92 ⁴. These findings supported the concept of a specific miRNAs signature in solid tumors ⁵. Indeed, a growing number of miRNAs, such as those of the let-7 and miR-34 families or the cluster miR-17-92 have been demonstrated to target genes that play an important role in lung carcinogenesis ⁶.

Although much progress concerning our understanding of miRNA function has been made, the identification of their targets still remains a limiting and difficult step ^{7,8}. In the current molecular framework, mature miRNA, charged into a complex called miRISC, which contains proteins of the Argonaute family ⁹, interact with complementary site(s), often located in the 3'-untranslated region (UTR) of a target mRNA. The current paradigm states that the interaction between the miRNA and its targets stems from a short stretch of 6-8 nucleotides located 5' of the miRNA, termed the “seed sequence” ¹⁰⁻¹². Consequently, one miRNA can theoretically target hundreds of mRNAs. Recent advances using high-throughput sequencing of RNAs have confirmed the wide range of miRNA action *in vivo* ¹³. miRISC complexes can relocate target mRNAs to specialized compartments, the P-bodies, where translation blockade or mRNA decay occur ¹⁴. Destabilization

of mRNA induced by miRNA is substantiated by many studies. Combined with computational predictions, measurement of expression profiles for mRNAs represents a powerful approach to identify functional miRNA-target relationships¹⁵⁻¹⁹.

We analyzed here the expression of miRNAs in a panel of biopsies of human Non-Small Cell Lung Carcinomas (NSCLC) according to their stages. This approach revealed peculiar expression of miR-210, which was preferentially detected in late-stage tumors. Recent studies have identified miR-210 among a set of hypoxia-regulated miRNAs and demonstrated the direct regulatory role of Hypoxia-Inducible Factor-1 alpha (HIF-1 α) in its transcription²⁰⁻²⁴. Contradictory data however exist concerning the regulation and roles of miR-210 during cancer progression. MiR-210 appears to be overexpressed in some solid tumors (breast, pancreas, gliomas, melanomas, head and neck carcinomas)^{21, 25-28} but absent in ovarian carcinoma²³. Furthermore, it has been shown that depending on the tissue type or cellular model, miR-210 was able to either promote entry into the cell cycle²⁸ and to inhibit apoptosis^{20, 22} or rather to repress tumor initiation²⁷. Several miR-210 targets have been investigated more specifically in the context of cancer, including cell cycle regulator *E2F3*²³, DNA repair factor *RAD52*²⁹, a member of the Fibroblast Growth Factor Receptor family (*FGFR1*), homeobox proteins (*HOXA1*, *HOXA9*)²⁷, the myc antagonist *MNT*²⁸, and the Iron Sulfur Cluster Assembly Proteins *ISCU1/2*³⁰, which are involved in many cellular processes such as heme biosynthesis and iron metabolism. However, the function of this miRNA is still poorly characterized.

In this study, we found that miR-210 was overexpressed at late stages of Non-Small Cell Lung Cancer (NSCLC). We next analyzed its function in the adenocarcinoma cell line A549 and provided evidence that miR-210 induced mitochondrial alterations associated with HIF-1 activation.

Results

MiR-210 is highly expressed at a late stage of lung cancers.

MiRNA expression was analyzed in 20 pairs (i.e. pathological versus matched control tissues from the same patient) of human primary lung adenocarcinoma and squamous cell carcinoma, using methods described elsewhere^{19, 31}. The clinical characteristics of these NSCLC specimens are listed in Table S1. We identified 33 miRNAs of interest, 13 being common with the study of Yanaihara *et al.*⁴ (Table S2). Fig.1A shows a heat map where the columns represent these 20 pairs of miRNA samples (tumor *versus* control) split into 3 groups according to their TNM staging and where the rows correspond to the selection of these 33 miRNAs supplemented with 13 additional miRNAs previously described for this pathology, such as members of the let-7 and the miR-34 families. We also looked at individual miRNAs the expression of which would differ during disease progression. We found 3 miRNAs with such a profile: miR-31, miR-210 and miR-451. While miR-21, a well-known oncogenic miRNA present in most epithelial malignancies was already found overexpressed at an early stage, higher expression of miR-210 and miR-31, and lower expression of miR-451 was usually associated with late stages of the disease (Fig. 1A). We then focused our attention on one of these candidates, the HIF-1-regulated miR-210, based on previous reports suggesting a strong association between hypoxia and poor outcome in NSCLC^{32, 33}.

MiR-210 expression correlates with a hypoxic signature in NSCLC and is up-regulated by hypoxia *in vitro*.

To compare miR-210 expression with a hypoxic signature, we first established the mRNA expression profiles of a subset of 13 biopsies from our initial NSCLC samples. The expression

values of 15 transcripts corresponding to a highly prognostic hypoxia signature (consisting of a small number of topranked hypoxic genes, including VEGFA, SLC2A1 and PGAM1) derived from a large meta-analysis of multiple cancers including lung cancer ³⁴ was used to set up a hypoxic index. The miR-210 levels in tumors showed positive correlation to this hypoxic index (Fig. 1B and Table S3). Finally, using TaqMan qRT-PCR, miR-210 was significantly induced in A549 cells under hypoxic condition (Fig. 1C), and this hypoxic induction was dependent on HIF1 α but not HIF2 α (Fig. S1) as previously reported in other models ^{27, 35}.

MiR-210 alters cell viability and enhances caspase 3/7 activity in A549 cells in normoxia.

Giannakakis et al, using several bioinformatic predictions of miRNA targets, reported that miR-210 can target the E2F family protein E2F3 ²³. Interestingly, E2F3 has also been identified as a target for the p53-regulated miR-34a ³⁶. Since miR-34a was also found slightly upregulated in some patients (Fig.1A) and identified as a prognostic marker of relapse in NSCLC ³⁷, we compared the effect of miR-210 with miR-34a and a siRNA against E2F3 (si-E2F3) on E2F3 expression. MiR-210 transfection led to a strong decrease in E2F3 protein expression (Fig. 2A). A luciferase reporter assay with the E2F3 3'UTR fused to luciferase showed that miR-210 directly targets E2F3 (Fig. 2B). We then compared ectopic expression of miR-210, miR-34a and si-E2F3 on A549 cell viability and proliferation using the XTT cell proliferation assay. After a transfection with miR-210 and si-E2F3, the number of A549 cells decreased over 5 days compared to the control (miR-Neg and si-Neg) (Fig. 2C). Meanwhile, A549 cells transfected with miR-34a escaped inhibition after 3 days. Interestingly, cell cycle analysis indicated that, in contrast to si-E2F3 and miR-34a, transfection with a pre-miR-210 increased the fraction of cells in sub G1 after 4 days of transfection, indicative of massive cell death (data not shown). This was confirmed by the caspase 3/7 activity, which revealed significant induction of apoptosis in A549

cells by miR-210 but not by si-E2F3 or miR-34a (Fig. 2D). The inhibitory effect of miR-210 on cell proliferation is therefore caused mainly by induction of apoptosis and clearly differs from the effect mediated by miR-34a and si-E2F3.

Identification of miR-210 targets by mRNA profiling of A549 cells overexpressing miR-210.

The influence of miR-210, miR-34a and si-E2F3 on transcript levels was investigated with human pan genomic arrays³⁸. Ectopic expression of miR-210 and miR-34a induced very different patterns of modulations (Fig. 3A; see Table S4 for the complete list of miR-210 deregulated transcripts). Moreover, a large number of changes induced by si-E2F3 were shared with miR-34a but not with miR-210 (Fig. 3A group 2), suggesting that miR-210 acts probably through a distinct mechanism. A functional annotation of the different signature patterns with the Ingenuity PathwayTM software was then performed. While there was an important overlap for “Molecular functions” terms such as “Cell Death”, “Cellular Growth and Proliferation” or “Cell Cycle” between miR-210, miR-34a and si-E2F3 (Table S5), we found some “canonical pathways” specific to one or the other experimental conditions (Table S6). As expected, the most significant pathway associated with miR-34 was “p53 signalling” ($p= 3.7 \cdot 10^{-7}$). The score of several metabolic pathways altered by the presence of miR-210 (namely: “Ascorbate and Aldarate Metabolism”, “Pyruvate Metabolism” and “Glutamate Metabolism”), was explained by its effects on several genes encoding aldehyde dehydrogenases, but we also noticed enrichment for a pathway related to “Mitochondria Dysfunction” (Table S6). This particularly interesting latter observation was explained by down-regulation of several members of complexes I and II of the Electron Transport Chain (ETC) (Fig. S2).

We next looked for putative miR-210 direct targets in the population of down-regulated transcripts using our web tool “MicrotopTable” (Fig. 3B-C)¹⁹. They indicate a specific over-

representation of miR-210- and miR-34a-predicted targets in the transcripts downregulated after heterologous expression of both miRNAs. While Fig. 3B-C are based on a target prediction by the TargetScan algorithm, similar conclusions were made when simply taking a “seed” match in the 3’UTR. Indeed, an about five-fold enrichment for the presence of the 6-nucleotide sequence (“CGCACA”) matching to the miR-210 “seed” was detected (Fig. 3D). We then focussed our analysis on 38 transcripts containing miR-210 complementary hexamers in their 3’UTR that show the largest inhibition of expression (Table 1). When this set of genes was functionally annotated, we found an enrichment for mitochondrial components (Table S7), explained in part by the presence of 2 members of ETC complexes: NADH dehydrogenase (ubiquinone) 1 alpha subcomplex, 4 (*NDUFA4*), a subunit of ETC complex I and succinate dehydrogenase complex, subunit D (*SDHD*), a subunit of the ETC complex II.

MiR-210 directly targets *NDUFA4* and *SDHD* and induces mitochondrial dysfunctions.

To test whether *NDUFA4* and *SDHD* were directly targeted by miR-210, we fused the 3’UTR of *SDHD* and *NDUFA4* to a luciferase reporter. Co-transfection with a synthetic pre-miR-210 significantly decreased the luciferase activity compared with a pre-miR-Neg, strongly suggesting that both genes are miR-210 targets (Fig. 4A). In the absence of specific antibodies against these 2 proteins, we performed western blot analysis on other subunits of these 2 ETC complexes (Fig. 4B). MiR-210 decreased the level of expression of the 70 kDa ETC complex II subunit (*SDHA*) but it had no impact on the 39 kDa ETC complex I subunit (*NDUFA9*) and the 20 kDa ETC complex I (*NDUFS7*). Finally, the activity of ETC complex II was directly measured on cell lysates of A549 cells, 72 hours following transfection with a pre-miR-Neg or pre-miR-210. MiR-210 specifically decreased SDH complex II activity compared to the miR-Neg control (Fig. 4C). Electron microscopy performed on miR-210-transfected A549 cells revealed mitochondrial

structural alterations (Fig. 4D): while the morphology of mitochondria in pre-miR-Neg transfected A549 cells appeared as a tubular network with normal internal membrane invaginations, miR-210 expressing cells showed enlarged mitochondria with a modified organization of cristae. These changes were visualized after 72 hours of transfection and this phenotype remained stable up to 5 days following treatment with miR-210. These phenotypic modifications were indeed associated with mitochondrial dysfunctions, as evidenced by an altered mitochondrial membrane potential ($\Delta\Psi_m$) (Fig. S3A).

The direct effect of miR-210 on SDHD was then assessed with a si-RNA targeting SDHD (si-SDHD). Silencing of SDHD with 2 different siRNAs mimicked the enlarged mitochondrial phenotype observed with miR-210 (Fig. 5A and S3B). Both si-SDHD and miR-210 induced a significant decrease in metabolically active cells 4 and 5 days following the treatment (Fig. 5B). Finally, the activity of caspase-3 and -7 was also increased by miR-210, and by si-SDHD, although to a lower extent (Fig. 5C).

Effects of miR-210 on cell survival and alteration in the phenotype of mitochondria in hypoxia.

Because alteration in mitochondrial function can lead to different consequences on cell death and survival in normoxia or hypoxia, we next performed clonogenic assays in which miR-210 was overexpressed or knocked down under normoxic or hypoxic conditions. As expected, transfection of a LNA inhibitor of miR-210 (LNA-210) in hypoxic A549 cells reduced miR-210 expression to the low basal normoxic level when compared to a LNA-159s control inhibitor (Fig. 6A). While transfection with a synthetic pre-miR-210 reduced clonogenic potential in normoxia (Fig. 6B, left), in agreement with our previous data on apoptosis and cell proliferation (Fig.2 and Fig. 4), treatment with LNA-210 resulted in decreased clonogenic survival of A549 cells following 72

hours of hypoxia (Fig. 6B, right). We also quantified in the same experimental settings, alterations in the mitochondrial phenotype as visualized by electron microscopy, which showed that LNA-210 could indeed significantly increase the average number of cristae under hypoxic conditions (Fig. 6C).

miR-210 positively regulates HIF-1 α activity.

Because mutations in SDH subunits have been shown to activate HIF-1^{39, 40}, we next wondered whether miR-210 had a positive effect on HIF-1 activity. As controls, we also evaluated the effect of miR-34a as well as those of si-E2F3 and si-SDHD. We measured their impact on several luciferase reporter vectors downstream to a minimal promoter containing either E2F, p53 or a hypoxia responsive element (HRE) (Fig. S4). As expected, both miR-210 and miR-34a duplexes as well as si-E2F3 induced a decrease in E2F reporter activity (Fig. S4A), while miR-34a duplex alone could increase p53 reporter activity (Fig. S4B). Of note, prolonged overexpression of the miR-210 duplex as well as silencing of SDHD resulted into a modest but significant increase of HRE luciferase reporter activity, suggesting that miR-210-mediated SDHD targeting leads to HIF-1 α stabilization under normoxic conditions (Fig. S4C). We next evaluated the level of expression and activity of HIF-1 α in experiments where miR-210 was overexpressed or knocked down under normoxic or hypoxic conditions (Fig. 7). Overexpression of miR-210 in normoxic conditions only led to a slight increase in HIF-1 α levels 72 hours after transfection (Fig. 7A), in agreement with the HRE luciferase reporter data (Fig. S4C). Importantly, inhibition of miR-210 in hypoxia decreased HIF-1 α proteins levels after 48-72 hours of hypoxia (Fig. 7A). After 48 hours of hypoxia, HIF-1 activity, as assessed after cotransfection of a HRE luciferase reporter, was reduced by LNA-210, and returned to basal values observed during normoxia (Fig. 7B).

Finally, the LNA-210 also reduced hypoxia-mediated lactate production to a similar extent as a si-RNA against HIF-1 α (Fig. 7C).

DISCUSSION

The main objective of this study was to analyze the regulation and function of miR-210 that was found upregulated in a cohort of 20 NSCLC. We provide evidence that miR-210 targets specific mitochondrial components with consequences on the regulation of cell death and survival and the modulation of HIF-1 activity through a positive regulatory loop *via* destabilization of the mitochondrial complex II activity (Fig. 7D).

The global miRNA profile reported here (Fig. 1) is in good agreement with previous reports^{4, 5}, showing up-regulation of miR-21, miR-155, miR-146a and miR-210 and repression of miR-125a, miR-143, miR-145 and miR-218. Stratification of the samples according to their stages revealed distinct levels of expression for miR-31, miR-210 and miR-451 among these groups. The low level of expression of miR-210 during early stages (1A, T1N0) and its progressive increase with growth and invasion of tumor cells fits well with previous reports showing a correlation between the well-characterized HIF-target carbonic anhydrase IX (CAIX), hypoxia and advanced T stage³². A link between miR-210 expression and aggressiveness has been suggested elsewhere in breast^{21, 25} and pancreatic tumors²⁶. A good correlation was also noted between miR-210 expression and hypoxic markers in our cohort of patients, confirming that miR-210 expression was likely driven by hypoxia *in vivo*, as previously shown in breast, head and neck tumor samples^{21, 27}. However, we found in few samples a detectable level of miR-210 without significant levels of hypoxic markers, suggesting that miR-210 may also be present under normoxic conditions. Several hypothesis can be proposed to explain this observation such as an induction *via* a HIF-independent pathway, increased copy numbers at this locus or a long-lasting upregulation following hypoxia. Further investigation need to be performed to answer to this question.

In an effort to better understand the function of miR-210 in lung tumor cells, we have first analyzed the consequences of miR-210 overexpression in A459 adenocarcinoma cells cultured under normoxic condition. Induction of apoptosis by miR-210 is consistent with very recent reports indicating that miR-210 represses the growth of tumor xenograft from both head, neck and pancreatic cancer cells ²⁷ and increases apoptosis in pulmonary arterial endothelial cells (HPAECs) *in vitro* ³⁰. While we confirmed that E2F3, a key protein in the cell cycle, is a functional target of miR-210 ²³, we also found that miR-210 induced cell death associated with activation of caspases, while E2F3 siRNA did not. Indeed, E2F3 silencing and miR-210 overexpressions led to very distinctive expression patterns, thus suggesting that the effect of miR-210-induced cell death was rather mediated by targeting other transcripts.

Among the set of transcripts that were down-regulated after ectopic expression of miR-210, we restricted our work to a group of 38 transcripts containing miR-210 complementary hexamers in their 3'UTR and possessing the strongest modulation factors and statistical *p*-values. Several transcripts of this list have already been identified in others cell types using a similar approach (*SYBL1*, *LASPI*, *SDF2*, *LHFP*, *TERF2IP*, *TNPO3*, *FAM3C*) ²⁸. We also found a validated miR-210 target, *HOXA1*, previously reported after immunoprecipitation of the Argonaute 2 (AGO2) protein coupled with DNA microarray analysis ²⁷. Finally, 18 additional miR-210 predicted targets described elsewhere ^{27, 28, 41}, including the recently validated gene *ISCU* ³⁰ were also identified after relaxing the log₂ ratio cut-off to -0.5, comforting our methodological approach. Its general applicability requires that the level of expression obtained after transfection remains in a “physiological” role. Otherwise, an abnormally high level of expression of miR-210 might induce adverse effects through alteration of “low affinity” targets. This is probably not the case here, since a final concentration of 0.1 nM of miR-210 was already able to induce A549 apoptosis (data not shown). Such a low concentration of miRNA duplex is also sufficient to induce similar

alterations of the transcriptome ¹⁹. Overall, combining microRNA transfection with expression studies definitely provides a useful complement to pure computational predictions. It remains that the list of proposed miRNA targets always requires a direct validation by Western blot analyses and/or reporter plasmid assays.

Functional annotations of the miR-210 overexpression experiments related miR-210 to “Mitochondria Dysfunction”, in line with the downregulation at mRNA level of several members of the complexes I and II of the Electron Transport Chain (ETC). Because HIF-1 α , the master regulator of the hypoxic response, has been shown to repress mitochondrial respiration ⁴², we then focused on two components: one subunit of ETC complex I, NDUFA4, and one of the four subunits of complex II, SDHD. Our model indicates that miR-210-mediated down-regulation of these ETC components could participate in HIF-1-induced mitochondrial dysfunction. Electron microscopy experiments support strongly this hypothesis (Fig. 4D and 5A), showing enlarged mitochondria with a modified organization of cristae in miR-210 expressing cells. These phenotypic modifications were associated with a decrease in the $\Delta\Psi_m$, consistent with our observation of an induction of apoptosis.

While the direct validation of these two targets was handicapped by the absence of specific antibodies against NDUFA4 and SDHD, we used three complementary approaches: i) 3'UTR luciferase constructs; ii) western blotting of other subunits of these two complexes; iii) the activity of the 2 complexes. Although a NDUFA4 3'UTR luciferase construct displayed significant inhibition by miR-210, we did not detect any effect of miR-210 at the protein level on other components nor on the activity of ETC complex I. This contrasted with SDHD, the fourth subunit of mitochondrial complex II, and also succinate dehydrogenase (SDH) of the TCA cycle, for which decreased expression and activity were noticed. It has been shown that mutations in SDH subunits including SDHD were linked with cancer and in particular lead to the development

of paragangliomas or pheochromocytomas^{43, 44}. A known consequence of the functional loss of any of these subunits is a great reduction of the enzymatic activity of the whole complex and a possible destabilization of the whole respiratory chain. Accordingly, miR-210 overexpression reduced the level of the SDHA subunit and of SDH activity. MiR-210 also inhibited the luciferase activity of a 3'UTR SDHD luciferase construct. SDHD inhibition mimicked several miR-210-mediated cellular effects, including alteration of mitochondrial ultrastructure (Fig. 5A), decrease of cell viability (Fig. 5B) and activation of caspases (Fig. 5C). Overall, these data are in perfect agreement with previous reports describing the consequences of SDHD mutations in paraganglioma, associated in particular with an unusual mitochondria phenotype^{45, 46}.

Our findings appear particularly interesting in the light of the report published during the preparation and revision of this manuscript^{30, 35, 47}, showing that miR-210 also targets ISCU1/2 proteins. ISCU1/2 facilitate the assembly of iron-sulfur clusters that are incorporated into enzymes involved in energy production, including mitochondrial respiratory complexes I, II and III. Chan *et al.* provided evidence that the lower levels of expression of ISCU1/2 mediated by miR-210 contribute to a decrease in the activity of the TCA cycle (through aconitase targeting) and the ETC (through complex I destabilization). Further studies will be necessary to dissect the relative importance of ISCU1/2 and SDHD on miR-210 function but it is already tempting to speculate that some synergy exists between both mechanisms.

The regulation of these mitochondrial components by the miR-210 pathway appears to have contrasting consequences on the regulation of cell death and survival under normoxic or hypoxic conditions. Indeed, clonogenic assays performed in either condition revealed that while overexpression of miR-210 reduced clonogenic potential in normoxia, treatment with LNA-210 resulted in decreased clonogenic survival in hypoxia (Fig. 6B). These apparently contradictory results highlight the complex processes involved in the regulation of mitochondrial respiration

and energy production in the hypoxic cell ⁴⁸. Based on this model, miR-210 overexpression in normoxia would create a mitochondrial dysfunction including a mismatch in electron transport that could lead notably to an increase in toxic ROS as recently suggested ³⁵ and increased apoptosis as corroborated by our data (Fig. 2D, Fig. 5 B-C). In contrast, during hypoxia, the miR-210-dependent repression of the ETC *via* SDHD, NDUFA4 or ISCU1/2 and other validated or yet unknown targets would be protective by participating in the homeostatic down-regulation of mitochondrial respiration. Notably, these effects can be recapitulated in clonogenic assays (Fig. 6B) and are in agreement with similar data published during revision of this manuscript ³⁵. Overall, these data strongly suggest that while miR-210 exerts a maladaptive role in normoxia, its induction following hypoxia would in contrast be protective, as suggested by other studies ^{22, 30, 49}.

Because the respiratory chain is not only involved in energy transfer but also serves as an intracellular O₂ sensor, miR-210-mediated targeting of SDHD is likely to have direct functional consequences on HIF-1 α activation. This molecular mechanism may play a role in the regulation of the phenomenon of increased glycolysis in tumors, known for decades as the “Warburg effect” ⁴². The link between the loss of mitochondrial tumor suppressors and pseudo-hypoxia (i.e. activation of HIF in the absence of a deficiency in oxygen) was indicated by several studies showing that SDH subunit mutations were linked with HIF-1 activation in highly vascularised tumors such as paragangliomas and pheochromocytomas ⁵⁰. Of note, microarray analysis of these SDH subunit-deficient tumors (including SDHD) revealed a HIF signature identical to that of a group of von Hippel-Lindau (VHL)-deficient tumors ⁴⁰. The VHL tumor suppressor is a key mediator of HIF activity, mediating ubiquitination and subsequent proteasome-mediated degradation of HIF α following its hydroxylation by HIF Prolyl Hydroxylase Domain proteins (PHD1, 2 or 3) in normoxia ⁵¹. Importantly, it has been shown that feedback inhibition of PHDs

by succinate, a product of PHDs, leads to HIF1- α stabilization⁵². Our findings showing that both miR-210 overexpression and SDHD silencing increase HRE luciferase activity are in perfect agreement with these data.

Moreover, another level of interplay has been proposed where HIF-1 is also able to down-regulate components of the mitochondrial complex II⁴⁰. Our findings suggest that miR-210 could explain this observation and be part of an autoregulatory loop, whereby HIF-1 contributes to attenuation of SDHD levels, leading to complex II inhibition, accumulation of succinate and resulting in blockade of HIF-1 α degradation. In agreement with this hypothesis, miR-210 inhibition reduced both the duration of HIF activation and lactate production in hypoxia (Fig. 7). The precise impact of the miR-210 / SDHD interaction in a hypoxic environment on HIF activity remains to be studied in detail as well as its consequences on mitochondria ultrastructure, function and cell death. A comprehensive understanding of the action of miR-210 will require integrating its multiple targets into a complex framework affecting cell cycle, cell migration, metabolic pathways, apoptotic potential and ROS production.

In conclusion, we have identified here SDHD as a direct target of miR-210 in A549 lung adenocarcinoma cells, thus revealing a positive regulatory loop associating miR-210 and HIF-1 α . Histological and functional evidences show that miR-210 exerts a major influence on mitochondrial function, cell survival and homeostasis. These data will now be further explored in light with other miR-210 targets to analyze its precise impact on hypoxia-related diseases including cancer.

Materials and methods

Clinical samples

Twenty pairs of primary NSCLC and corresponding non-cancerous lung tissues were obtained from patients in Nice (France) and collected by the Tumor Biobank of the Nice hospital (www.biobank06.com/, agreement LPB04/LPB05). All patients signed an informed consent sheet for this study. Clinical and pathological data are described in Table S1.

Cell culture

The lung adenocarcinoma A549 cell line was purchased from the American Type Culture Collection and were grown in DMEM supplemented with L-glutamine and 10 % FBS at 37°C in a humidified 5 % CO₂ air atmosphere. A Bug-Box™ anaerobic workstation (Ruskin Technology) set at 1% oxygen, 94% nitrogen and 5% carbon dioxide was used for hypoxic conditions.

RNA isolation

Frozen tissue (~50 mg) from clinical samples was pulverized in a stainless steel mortar and pestle. Total RNA was extracted from the samples with TRIzol™ solution (Invitrogen), and the integrity of RNA was assessed by using an Agilent BioAnalyser 2100 (Agilent, RIN above 6.5). RNA concentration was determined using the ND-1000 micro-spectrophotometer (NanoDrop Technologies). The miRvana™ miRNA isolation kit was used for isolation and enrichment of small RNA fractions (Ambion), according to the manufacturer's protocol.

Quantitative RT-PCR of mature miRNA

MiR-210 expression was evaluated using TaqMan MicroRNA Assay (Applied Biosystems) as specified in their protocol. Real-time quantitative PCR was performed using GeneAmp Fast PCR Master Mix (Applied Biosystems) and Lightcycler 480 (Roche) real-time PCR machine. All reactions were performed in duplicate. Expression levels of mature microRNAs were evaluated using comparative CT method (2-deltaCT). Transcript levels of RNU6B were used as endogenous control.

Transfection

Chemically synthesized miRNA duplexes, called pre-miR-210, pre-miR-34a and control miRNA (pre-miR-Neg # 1) were purchased from Ambion; for miR-210 knockdown experiments, anti-miR-210 LNA and negative control anti-miR-159s LNA (miRCURY LNA Knockdown probes) were ordered from Exiqon. Si-RNAs directed against E2F3, SDHD and NDUFA4 were from Applied Biosystems. A549 cells were transfected at 50% confluency with Lipofectamin RNAi MAXTM (Invitrogen) and with pre-miRNA, siRNA or the LNA inhibitor at a final concentration of 10 nM.

Molecular constructs

Molecular constructs were made in pSI-CHECKTM-2 (Promega) by cloning behind the *Renilla* luciferase in the *XhoI* and *NotI* restrictions sites, 3'UTR sequences from E2F3, NDUFA4 and SDHD mRNA and named as pSI-E2F3-1 (containing the miR-210 binding site), pSI-E2F3-2 (containing the miR-34a binding site), pSI-NDUFA4 and pSI-SDHD respectively. A positive control for miR-210 was created by cloning a miR-210 complementary sequence in *XhoI/NotI* restriction sites in pSI-CHECK-2 (Promega) and named as pSI-miR-210.

hsa-E2F3-1 / sense: ACTACTCGAGGTGTTGTCCCTTCCTACCTTCTT

hsa-E2F3-1 / reverse: ATAAGAATGCGGCCGCGCACATTTTCTCACTTGCTGAC

hsa-E2F3-2 / sense: CCGCTCGAGGCTGCTATTAAAGCTCACACACGAA

hsa-E2F3-2 / reverse: ATAAGAATGCGGCCGCGCACGAGTTGTCATGCACACACTGAA

hsa-SDHD / sense: GGTGGACAGCCTTCTTCTCTTAATC

hsa-SDHD / reverse: CATAGAATACATTTTCACATTAGAGATTCCC

hsa-NDUFA4 / sense: GAAATGTTTCACTATAACGCTGCTTTAG

hsa-NDUFA4 / reverse: GCCAGTGTCAGATGCTGGAG

miRNA targets validation by luciferase assay

Co-transfection of 200 ng pSI-CHECKTM-2 with 10 nM of pre-miRNA was carried out in 96-well plates with Lipofectamine 2000 (Invitrogen). Transfection of the same combinations of plasmid and RNAs were repeated three times in HEK293 (data not shown) and A549 cells. The medium was replaced 8 hours after transfection with fresh medium containing 10% FCS, L-glutamine and supplemented with penicillin and streptomycin. 48 hours after transfection, firefly and *Renilla* Luciferase activities were measured using the Dual-GloTM Luciferase assay (Promega).

Cell proliferation assay

A549 cells were plated at $3 \cdot 10^3$ cells per well in 96-well plates with triplicate wells for each transfection. Cell proliferation was performed using the XTT colorimetric assay (Cell proliferation assay kit II, Roche). After two to five days of transfection with pre-miRNAs or siRNAs, 50 μ l of XTT labeling mixture was added to each well, and incubation was continued

for 2 hours. Cell viability was assessed by measuring the absorbance at 490 nm using a microtiter plate (ELISA) reader.

Caspase 3/7 assay

The activation of executioner caspase-3 and -7 in A549 cells was determined using the Caspase-Glo 3/7 Assay kit (Promega) according to manufacturer's instructions. A549 cells were plated in triplicate in 96-well plates and transfected as described above. Luminescence was quantified after 1 hour of incubation with the caspase substrate on a luminometer .

Western blot analysis

Cells were lysed in 1.5 x Laemmli buffer and the protein concentration determined using the BCA assay. In the case of E2F3, nuclear extracts were made using the NE-PER kit (Pierce). 40 µg of protein of whole cell extracts was resolved by SDS-PAGE and transferred onto a PVDF membrane (Millipore). Membranes were blocked in 5% non-fat milk in TN buffer (50 mM Tris-HCl pH 7.4, 150 mM NaCl) and incubated in the presence of the primary and then secondary antibodies in 5 % non-fat milk in TN buffer. After washing in TN buffer containing 1 % Triton-X100 and then in TN buffer, immunoreactive bands were visualized with the ECL system (Amersham Biosciences). Antibodies to E2F3 (N-20), total ERK2 and α -Tubulin were purchased from Santa Cruz, to NDUFA9 and SDHA from Invitrogen, to HDAC1 from Neomarker. The rabbit polyclonal anti-HIF-1 α antibody (antiserum 2087) has been reported previously ⁵³.

Transmission Electronic Microscopy

Cells were fixed *in situ* with 1.6% glutaraldehyde in 0.1 M phosphate buffer at room temperature for at least one hour and then conserved at 4 °C. Samples were rinsed in the same buffer then

post-fixed with 1% osmium tetroxide and 1% potassium ferrocyanide in 0.1 M cacodylate buffer for 1 hour at RT to enhance the staining of cytoplasmic membranes. Cells were rinsed with distilled water and embedded in epoxy resin. Embedded samples were then processed for thin sectioning and observed with a JEM1400 transmission electron microscope (Jeol) equipped with a Morada CCD camera (Olympus SIS).

Microarrays

MiRNA microarrays. The oligonucleotide sequences corresponding to 2054 mature miRNAs (including 409 *Homo sapiens*) found in the miRNA registry (Release 8.2;⁵⁴) are available on <http://www.microarray.fr:8080/merge/index> (follow the link to “microRNA”: platform referenced in GEO as GPL4717 and GPL4718). The experimental data and microarray design have been deposited in the NCBI Gene Expression Omnibus (GEO) (<http://www.ncbi.nlm.nih.gov/geo/>) under serie GSE18692. The experimental design used a dye-swap approach, so that each human probe, printed 8 times on the microarray was measured independently 16 times for each sample. Target preparation and array hybridization were performed as previously described^{19,31}.

Expression microarrays. Pangenomic microarrays were printed using the human RNG/MRC oligonucleotide collection as previously described³⁸. RNA were labelled and hybridized as previously described¹⁹. Two biological replicates were performed for each comparison. The experimental data and microarray design have been deposited in the NCBI Gene Expression Omnibus (GEO) (<http://www.ncbi.nlm.nih.gov/geo/>) under serie GSE18694.

Statistical analysis. Normalization was performed using the Limma package available from Bioconductor (<http://www.bioconductor.org>). Intra slide and inter slide normalization was performed using the Print Tip Loess and the quantile methods, respectively. Means of ratios from all comparisons were calculated and B test analysis was performed. Differentially expressed

genes were selected using Benjamini-Hochberg correction of the p -value for multiple tests, based on a p -value below 0.01.

Biological Theme Analysis. Data from expression microarrays were analyzed for enrichment in biological themes (Gene Ontology molecular function and biological process) and build biological networks built using Ingenuity Pathway Analysis software (<http://www.ingenuity.com/>) and Mediante (<http://www.microarray.fr:8080/merge/index>)⁵⁵, an information system containing diverse information about our probes and data sets.

MiR-210 targets analysis. MicroTopTable is an online java web tool (available at <http://www.microarray.fr:8080/merge/index> follow the link to microRNA and Bioinformatic tools) that integrates DNA microarrays data to identify the potential implication of miRNAs on a specific biological system¹⁹. It allows a rapid characterization of the most pertinent mRNA targets according to several existing miRNA target prediction approaches: Targetscan, MicroCosm, Miranda, Pictar and an exact seed search (2-7, 1-8 or 2-8 first nucleotides of the miRNA). Briefly, MicroTopTable ranks the transcripts into 3 categories (“Upregulated”, “Down regulated” and “non-modulated”), according to thresholds for expression level and for differential expression. It then calculates the number of predicted targets for each miRNA, according to the prediction software selected, in each of the three categories. Enrichment in miRNA targets in each category is then tested using the hypergeometric function. Data obtained with MicroTopTable have been compared with the “Sylamer” approach⁵⁶ that confirmed overrepresentation of the same hexamers in our data set.

SDH assay

SDH activity was measured according to Gimenez-Roqueplo *et al.*³⁹. Cellular lysates were diluted to 0.2 mg protein/ml in 50 mM potassium phosphate buffer and pH 7.5 on ice. Sodium

succinate (20 mM), 2,6-dichloroindophenol (DCIP) (50 μ M), ATP (100 μ M) and potassium cyanide (1 mM) were added to a well of a 96-well plate. The cellular lysate (20 μ l) containing 4 μ g of protein was added to the well and the reaction was started by addition of 50 μ l decylubiquinone (0.4 mM). The decrease in absorbance at 600 nm was measured for 20 min at 37 °C. SDH activity was expressed as $\text{mmol} \cdot \text{min}^{-1} \cdot \text{mg}^{-1}$.

Flow cytometric analysis of mitochondrial membrane potential

Changes in the $\Delta\Psi_m$ were analyzed using the MitoProbe JC-1 assay kit (JC-1; MolecularProbes, Inc., Eugene, OR). This cyanine dye accumulates in the mitochondrial matrix under the influence of the $\Delta\Psi_m$ and forms J aggregates indicated by a fluorescence emission shift from green (~529 nm) to red (~590 nm). A549 cells transfected as described above were collected each indicated day and stained with 2 μ M of JC-1 in warm medium at 1×10^6 cells/ml during 30 min at 37 °C. The cells were washed by adding 2 ml of warm PBS, centrifugated and resuspended in 500 μ l PBS. As a positive control for reduction of $\Delta\Psi_m$, A549 cells were treated with the uncoupling agent carbonyl cyanide m-chlorophenylhydrazone. Cell suspensions were prepared and flow cytometry was performed on a FACScalibur and analyzed using Cell quest (Becton–Dickinson Immunocytometry Systems). The ratio of green versus red fluorescence intensities was calculated.

Promoter reporter assay

Reverse transfection into A549 cells ($2 \cdot 10^4$ cell/well) were made in triplicate with 100 ng of a mixture of a transcription factor-responsive firefly luciferase construct “E2F, p53 or HIF Reporter” (Signal Finder™ Pathway Reporter Assays) and constitutively expressing *Renilla* luciferase construct (40:1) and 10 nM of miRNA or siRNA by Lipofectamine 2000 (Invitrogen).

A mixture of non-inducible firefly luciferase construct and constitutively expressing *Renilla* luciferase construct used as negative control and a mixture of constitutive expressing firefly and *Renilla* luciferase constructs used as positive control were also transfected. Sixteen hours post transfection, fresh medium with antibiotics was added and three to four days later, the activities of the signaling pathway E2F, p53 or HIF was measured with the Dual-Glo luciferase assay (Promega).

Determination of the extracellular lactate concentration.

The lactate concentration in the supernatant of cells incubated either in normoxia or in hypoxia of 1% O₂ for 48 hours was determined by an enzyme-based assay using 900 µM β-NAD (BioChemika), 175 µg/ml L-lactate dehydrogenase (BioChemika) and 100 µg/ml glutamate-pyruvate transaminase (Roche) diluted in a sodium carbonate (620 mM)-L-glutamate (79 mM) buffer adjusted to pH 10. Lithium lactate was used as a standard. Measurement was done with a microplate reader after incubation for 30 min at 37°C. For each condition, the protein concentration was determined to express the lactate concentration as mM/µg protein.

Colony Assays

Following transfection, A549 cells were placed in normoxia or hypoxia (1 % O₂) for 72 hours. Cells were then trypsinized, counted, re-plated at a density of 100 and 500 cells/well (2.5 cm²) and incubated during 11 days. Cells were then washed, fixed and stained. Images were background-subtracted and processed in *ImageJ* for CFU quantification. The surviving fractions were calculated based upon the plating efficiency.

Statistical analysis.

Results are given as the mean \pm S.E.M. Statistical analysis was performed using the Student's t-test as provided by Microsoft Excel™ and the null hypothesis was rejected at the 0.05 level (** $p < 0.0005$, ** $p < 0.005$, * $p < 0.05$).

ACKNOWLEDGMENTS:

We acknowledge the excellent support of the Nice-Sophia Antipolis Functional Genomics Platform in which the microarray experiments were carried out. The authors also thank Frédéric Brau and Julie Cazareth for excellent technical assistance concerning microscopy and flow cytometry experiments, and Karine Ilc for excellent technical assistance concerning IHC. We acknowledge Pr Mouroux and Pr Vénissac (Department of Thoracic Surgery, Pasteur Hospital, CHU of Nice, France) for providing us with surgical lung specimens, and Mr Eric Selva and Ms Virginie Tanga-Gavric (Human Biobank, CHU of Nice) for excellent technical assistance. We thank Patrick Auberger, Brice Marcet and Patricia L.M. Dahia for helpful discussion and Ms Christiane Brahimi-Horn for critical reading and editorial correction of the manuscript.

SUPPLEMENTAL DATA

Supplemental information is provided corresponding to seven tables and four figures.

References

1. Jemal A, Siegel R, Ward E, Hao Y, Xu J, Murray T *et al.* Cancer statistics, 2008. *CA Cancer J Clin* 2008; **58**(2): 71-96.
2. Harpole DH, Jr. Prognostic modeling in early stage lung cancer: an evolving process from histopathology to genomics. *Thorac Surg Clin* 2007; **17**(2): 167-73.
3. Lu J, Getz G, Miska EA, Alvarez-Saavedra E, Lamb J, Peck D *et al.* MicroRNA expression profiles classify human cancers. *Nature* 2005; **435**(7043): 834-8.
4. Yanaihara N, Caplen N, Bowman E, Seike M, Kumamoto K, Yi M *et al.* Unique microRNA molecular profiles in lung cancer diagnosis and prognosis. *Cancer Cell* 2006; **9**(3): 189-98.
5. Volinia S, Calin GA, Liu CG, Ambs S, Cimmino A, Petrocca F *et al.* A microRNA expression signature of human solid tumors defines cancer gene targets. *Proc Natl Acad Sci U S A* 2006; **103**(7): 2257-61.
6. Ortholan C, Puissegur MP, Ilie M, Barbry P, Mari B, Hofman P. MicroRNAs and lung cancer: new oncogenes and tumor suppressors, new prognostic factors and potential therapeutic targets. *Curr Med Chem* 2009; **16**(9): 1047-61.
7. Brodersen P, Voinnet O. Revisiting the principles of microRNA target recognition and mode of action. *Nat Rev Mol Cell Biol* 2009; **10**(2): 141-8.
8. Bartel DP. MicroRNAs: target recognition and regulatory functions. *Cell* 2009; **136**(2): 215-33.
9. Peters L, Meister G. Argonaute proteins: mediators of RNA silencing. *Mol Cell* 2007; **26**(5): 611-23.
10. Lewis BP, Burge CB, Bartel DP. Conserved seed pairing, often flanked by adenosines, indicates that thousands of human genes are microRNA targets. *Cell* 2005; **120**(1): 15-20.
11. Brennecke J, Stark A, Russell RB, Cohen SM. Principles of MicroRNA-Target Recognition. *PLoS Biol* 2005; **3**(3): e85.
12. Doench JG, Sharp PA. Specificity of microRNA target selection in translational repression. *Genes Dev* 2004; **18**(5): 504-11.
13. Chi SW, Zang JB, Mele A, Darnell RB. Argonaute HITS-CLIP decodes microRNA-mRNA interaction maps. *Nature* 2009; **460**(7254): 479-86.
14. Filipowicz W, Bhattacharyya SN, Sonenberg N. Mechanisms of post-transcriptional regulation by microRNAs: are the answers in sight? *Nat Rev Genet* 2008; **9**(2): 102-14.

15. Lim LP, Lau NC, Garrett-Engele P, Grimson A, Schelter JM, Castle J *et al.* Microarray analysis shows that some microRNAs downregulate large numbers of target mRNAs. *Nature* 2005; **433**(7027): 769-73. Epub 2005 Jan 30.
16. Rodriguez A, Vigorito E, Clare S, Warren MV, Couttet P, Soond DR *et al.* Requirement of bic/microRNA-155 for normal immune function. *Science* 2007; **316**(5824): 608-11.
17. Huang J, Liang Z, Yang B, Tian H, Ma J, Zhang H. Derepression of microRNA-mediated protein translation inhibition by apolipoprotein B mRNA-editing enzyme catalytic polypeptide-like 3G (APOBEC3G) and its family members. *J Biol Chem* 2007; **282**(46): 33632-40.
18. Baek D, Villen J, Shin C, Camargo FD, Gygi SP, Bartel DP. The impact of microRNAs on protein output. *Nature* 2008; **455**(7209): 64-71.
19. Pottier N, Maurin T, Chevalier B, Puissegur MP, Lebrigand K, Robbe-Sermesant K *et al.* Identification of keratinocyte growth factor as a target of microRNA-155 in lung fibroblasts: implication in epithelial-mesenchymal interactions. *PLoS One* 2009; **4**(8): e6718.
20. Kulshreshtha R, Ferracin M, Wojcik SE, Garzon R, Alder H, Agosto-Perez FJ *et al.* A microRNA signature of hypoxia. *Mol Cell Biol* 2007; **27**(5): 1859-67.
21. Camps C, Buffa FM, Colella S, Moore J, Sotiriou C, Sheldon H *et al.* hsa-miR-210 Is induced by hypoxia and is an independent prognostic factor in breast cancer. *Clin Cancer Res* 2008; **14**(5): 1340-8.
22. Fasanaro P, D'Alessandra Y, Di Stefano V, Melchionna R, Romani S, Pompilio G *et al.* MicroRNA-210 modulates endothelial cell response to hypoxia and inhibits the receptor tyrosine kinase ligand Ephrin-A3. *J Biol Chem* 2008; **283**(23): 15878-83.
23. Giannakakis A, Sandaltzopoulos R, Greshock J, Liang S, Huang J, Hasegawa K *et al.* miR-210 links hypoxia with cell cycle regulation and is deleted in human epithelial ovarian cancer. *Cancer Biol Ther* 2008; **7**(2): 255-64.
24. Pulkkinen K, Malm T, Turunen M, Koistinaho J, Yla-Herttuala S. Hypoxia induces microRNA miR-210 in vitro and in vivo ephrin-A3 and neuronal pentraxin 1 are potentially regulated by miR-210. *FEBS Lett* 2008; **582**(16): 2397-401.
25. Foekens JA, Sieuwerts AM, Smid M, Look MP, de Weerd V, Boersma AW *et al.* Four miRNAs associated with aggressiveness of lymph node-negative, estrogen receptor-positive human breast cancer. *Proc Natl Acad Sci U S A* 2008; **105**(35): 13021-6.
26. Greither T, Grochola LF, Udelnow A, Lautenschlager C, Wurl P, Taubert H. Elevated expression of microRNAs 155, 203, 210 and 222 in pancreatic tumors is associated with poorer survival. *Int J Cancer* 2009; **126**(1): 73-80.

27. Huang X, Ding L, Bennewith KL, Tong RT, Welford SM, Ang KK *et al.* Hypoxia-inducible mir-210 regulates normoxic gene expression involved in tumor initiation. *Mol Cell* 2009; **35**(6): 856-67.
28. Zhang Z, Sun H, Dai H, Walsh RM, Imakura M, Schelter J *et al.* MicroRNA miR-210 modulates cellular response to hypoxia through the MYC antagonist MNT. *Cell Cycle* 2009; **8**(17): 2756-68.
29. Crosby ME, Kulshreshtha R, Ivan M, Glazer PM. MicroRNA regulation of DNA repair gene expression in hypoxic stress. *Cancer Res* 2009; **69**(3): 1221-9.
30. Chan SY, Zhang YY, Hemann C, Mahoney CE, Zweier JL, Loscalzo J. MicroRNA-210 controls mitochondrial metabolism during hypoxia by repressing the iron-sulfur cluster assembly proteins ISCU1/2. *Cell Metab* 2009; **10**(4): 273-84.
31. Triboulet R, Mari B, Lin YL, Chable-Bessia C, Bennasser Y, Lebrigand K *et al.* Suppression of microRNA-silencing pathway by HIV-1 during virus replication. *Science* 2007; **315**(5818): 1579-82.
32. Giatromanolaki A, Koukourakis MI, Sivridis E, Pastorek J, Wykoff CC, Gatter KC *et al.* Expression of hypoxia-inducible carbonic anhydrase-9 relates to angiogenic pathways and independently to poor outcome in non-small cell lung cancer. *Cancer Res* 2001; **61**(21): 7992-8.
33. Ilie M, Mazure NM, Hofman V, Ammadi RE, Ortholan C, Bonnetaud C *et al.* High levels of carbonic anhydrase IX in tumour tissue and plasma are biomarkers of poor prognostic in patients with non-small cell lung cancer. *Br J Cancer* 2010; **102**(11): 1627-35.
34. Buffa FM, Harris AL, West CM, Miller CJ. Large meta-analysis of multiple cancers reveals a common, compact and highly prognostic hypoxia metagene. *Br J Cancer* 2010; **102**(2): 428-35.
35. Favaro E, Ramachandran A, McCormick R, Gee H, Blancher C, Crosby M *et al.* MicroRNA-210 regulates mitochondrial free radical response to hypoxia and krebs cycle in cancer cells by targeting iron sulfur cluster protein ISCU. *PLoS One* 2010; **5**(4): e10345.
36. Tazawa H, Tsuchiya N, Izumiya M, Nakagama H. Tumor-suppressive miR-34a induces senescence-like growth arrest through modulation of the E2F pathway in human colon cancer cells. *Proc Natl Acad Sci U S A* 2007; **104**(39): 15472-7.
37. Gallardo E, Navarro A, Vinolas N, Marrades RM, Diaz T, Gel B *et al.* miR-34a as a prognostic marker of relapse in surgically resected non-small-cell lung cancer. *Carcinogenesis* 2009; **30**(11): 1903-9.

38. Le Brigand K, Russell R, Moreilhon C, Rouillard JM, Jost B, Amiot F *et al.* An open-access long oligonucleotide microarray resource for analysis of the human and mouse transcriptomes. *Nucleic Acids Res* 2006; **34**(12): e87.
39. Gimenez-Roqueplo AP, Favier J, Rustin P, Mourad JJ, Plouin PF, Corvol P *et al.* The R22X mutation of the SDHD gene in hereditary paraganglioma abolishes the enzymatic activity of complex II in the mitochondrial respiratory chain and activates the hypoxia pathway. *Am J Hum Genet* 2001; **69**(6): 1186-97.
40. Dahia PL, Ross KN, Wright ME, Hayashida CY, Santagata S, Barontini M *et al.* A HIF1alpha regulatory loop links hypoxia and mitochondrial signals in pheochromocytomas. *PLoS Genet* 2005; **1**(1): 72-80.
41. Fasanaro P, Greco S, Lorenzi M, Pescatori M, Brioschi M, Kulshreshtha R *et al.* An integrated approach for experimental target identification of hypoxia-induced miR-210. *J Biol Chem* 2009.
42. Denko NC. Hypoxia, HIF1 and glucose metabolism in the solid tumour. *Nat Rev Cancer* 2008.
43. Baysal BE, Ferrell RE, Willett-Brozick JE, Lawrence EC, Myssiorek D, Bosch A *et al.* Mutations in SDHD, a mitochondrial complex II gene, in hereditary paraganglioma. *Science* 2000; **287**(5454): 848-51.
44. Gottlieb E, Tomlinson IP. Mitochondrial tumour suppressors: a genetic and biochemical update. *Nat Rev Cancer* 2005; **5**(11): 857-66.
45. Robertson DI, Cooney TP. Malignant carotid body paraganglioma: light and electron microscopic study of the tumor and its metastases. *Cancer* 1980; **46**(12): 2623-33.
46. Douwes Dekker PB, Hogendoorn PC, Kuipers-Dijkshoorn N, Prins FA, van Duinen SG, Taschner PE *et al.* SDHD mutations in head and neck paragangliomas result in destabilization of complex II in the mitochondrial respiratory chain with loss of enzymatic activity and abnormal mitochondrial morphology. *J Pathol* 2003; **201**(3): 480-6.
47. Chen Z, Li Y, Zhang H, Huang P, Luthra R. Hypoxia-regulated microRNA-210 modulates mitochondrial function and decreases ISCU and COX10 expression. *Oncogene* 2010.
48. Semenza GL. Oxygen-dependent regulation of mitochondrial respiration by hypoxia-inducible factor 1. *Biochem J* 2007; **405**(1): 1-9.
49. Kulshreshtha R, Davuluri RV, Calin GA, Ivan M. A microRNA component of the hypoxic response. *Cell Death Differ* 2008; **15**(4): 667-71.
50. King A, Selak MA, Gottlieb E. Succinate dehydrogenase and fumarate hydratase: linking mitochondrial dysfunction and cancer. *Oncogene* 2006; **25**(34): 4675-82.

51. Kaelin WG. The von Hippel-Lindau tumor suppressor protein: roles in cancer and oxygen sensing. *Cold Spring Harb Symp Quant Biol* 2005; **70**: 159-66.
52. Selak MA, Armour SM, MacKenzie ED, Boulahbel H, Watson DG, Mansfield KD *et al.* Succinate links TCA cycle dysfunction to oncogenesis by inhibiting HIF-alpha prolyl hydroxylase. *Cancer Cell* 2005; **7**(1): 77-85.
53. Richard DE, Berra E, Gothie E, Roux D, Pouyssegur J. p42/p44 mitogen-activated protein kinases phosphorylate hypoxia-inducible factor 1alpha (HIF-1alpha) and enhance the transcriptional activity of HIF-1. *J Biol Chem* 1999; **274**(46): 32631-7.
54. Griffiths-Jones S. miRBase: the microRNA sequence database. *Methods Mol Biol* 2006; **342**: 129-38.
55. Le Brigand K, Barbry P. Mediante: a web-based microarray data manager. *Bioinformatics* 2007; **23**(10): 1304-6.
56. van Dongen S, Abreu-Goodger C, Enright AJ. Detecting microRNA binding and siRNA off-target effects from expression data. *Nat Methods* 2008; **5**(12): 1023-5.

Legends to Tables and Figures

Table 1. List of the miR-210-predicted targets down-regulated following miR-210 overexpression in A549 cells.

The 38 transcripts containing at least one complementary sequence to the “seed 2-7” of miR-210 in their 3'UTR and strongly repressed following miR-210 transfection are listed. Cut-offs for selection are equal to 8.0 for the \log_2 (signal), to -1 for the \log_2 (ratio), and to 0.001 for the adjusted *p*-value. Logarithm (base 2) of the ratio of miR-210/miR-Neg is represented. ID: corresponds to RNG oligo IDs that gives access to transcripts and probes annotations through our information system Mediante (<http://www.microarray.fr:8080/merge/index>).

Figure 1. Overexpression of miR-210 in NSCLC is linked to hypoxia induction in tumors.

(A) Unsupervised hierarchical clustering analysis of 42 miRNAs in 20 NSCLC samples. Distance was measured using the Manhattan distance on the matrix of the \log_2 (ratio) and classification was performed using a complete agglomeration method. Histograms on the right of the panel represents miR-210, miR-31 and miR-451 modulation in three different stages of the disease. (B) Expression of miR-210 and the hypoxic index in 13 NSCLC samples. Histograms represent the \log_2 ratio of tumor versus normal adjacent tissues for miR-210 and for a hypoxic index corresponding to the average value of the 15 top-ranked genes (see Table S3 for the list of the transcripts) of the common hypoxia metagene identified by Buffa et al.³⁴. Similar results were obtained with the full list of this common hypoxia signature. (C) MiR-210 expression was monitored by qPCR on RNA from A549 cells with or without exposure to 1% O₂ at indicated times. Mean \pm SEM is representative of 3 independent experiments carried out in triplicate.

Figure 2. MiR-210 targets E2F3 and alters A549 cell viability. (A) A549 cells were transfected with 10 nM pre-miR-210, premiR-34a, pre-miR-Neg, si-Neg or si-E2F3 as a positive control. E2F3 protein levels were determined by western blotting on day 2 post-transfection. HDAC1 expression was used as a loading control. (B) A549 cells were co-transfected with 10nM pre-miR-Neg, pre-miR-210 or pre-miR-34a and different pSI-Check-2TM constructs. Cells were harvested two days after transfection and the luciferase activities analyzed. All *Renilla* luciferase activities were normalized to the firefly luciferase activity. pSI-E2F3-1 and pSI-E2F3-2 correspond to distinct fragments of the *E2F3* 3'UTR containing putative miR-210 and miR-34a putative binding sites respectively, pSI-check2 was used as an empty vector control. (C) The XTT cell viability assay was performed on days 1 to 5 after transfection of A549 cells with pre-miR-Neg, pre-miR-210, pre-miR-34a, , si-Neg or si-E2F3 . (D) The caspase 3/7 assay was carried out on A549 cells transfected under the same conditions as in (C). Results correspond to 3 independent experiments performed in duplicate.

Figure 3. Identification of miR-210 candidate targets using a transcriptomic approach. A549 cells were transfected with pre-miR-Neg, pre-miR-210, pre-miR-34a as well as siE2F3 or a control siRNA (si-Neg) (n=2). RNA samples were harvested at 48 h post-transfection and expression profiles were determined with pan genomic arrays. (A) Heatmap comparing the normalized log₂ of the ratios between the signal in the different conditions and the pre-miR-Neg signal, 48 h after transfection. (B) and (C) Over-representation of miR-210 (B) and miR-34a (C) predicted targets according to TargetScan algorithm following transfection with pre-miR-210 and pre-miR-34a, respectively. Representation of miRNA predicted targets in the set of up- or down-

regulated genes was compared with the set of all expressed genes. For each miRNA, a fold enrichment value (horizontal axis) and an associated *P*-Value (vertical axis) were calculated. (D) Histogram representing the enrichment for the presence of seed complementary hexamers in the 3'-UTR of down- or up-regulated transcripts following transfection with pre-miR-210, pre-miR-34a and si-E2F3.

Figure 4. MiR-210 targets SDHD and induces mitochondrial dysfunction. (A) Direct targeting of SDHD and NDUFA4 by miR-210 *in vitro*. A549 cells were co-transfected with 10 nM of pre-miR-Neg, pre-miR-210 or pre-miR-34a with pSI-Check-2TM constructs containing the 3'UTR of SDHD (pSI-SDHD) or NDUFA4 (pSI-NDUFA4). Cells were harvested two days after transfection and luciferase activities were analyzed. (B) Effect of miR-210 expression on endogenous members of ETC complex I and II. The A549 cell line was transfected with 10 nM pre-miR-Neg, pre-miR-210 or pre-miR-34a. SDHA, NDUFA9 and NDUF57 protein levels were determined by western blotting on day 2 post-transfection. Total ERK2 was used as a loading control. (C) Complex II activity was performed on A549 cells day 3 post-transfection with pre-miR-Neg or pre-miR-210. (D) Electron micrographs of the ultrastructure of mitochondria of A549 cells transfected with miR-Neg or miR-210. All data are representative from 3 independent experiments.

Figure 5. SiRNAs directed against SDHD induce modifications in mitochondrial shape and apoptosis. (A) Mitochondrial ultrastructure in A549 cells transfected with pre-miR-Neg, pre-miR-210, si-Neg or two different si-SDHD alone or together and fixed *in situ* at 4 days after transfection. miR-210 and si-SDHD strongly modified mitochondrial structure (arrow). (B) XTT cell proliferation and (C) Caspase 3/7 assays were performed on A549 cells transfected with pre-

miR-Neg, pre-miR-210, , si-Neg or si-SDHD or. All data are representative from 3 independent experiments performed in triplicate.

Figure 6. MiR-210 inhibition decreases cell survival and affects the phenotype of mitochondria in hypoxia. A549 cells were transfected with either pre-miR-Neg, pre-miR-210, a control anti-miR-159s LNA or anti-miR-210, before 72-96 h exposure to normoxia or 1% O₂. A) MiR-210 expression was monitored by qPCR on RNA from A549 cells with or without exposure to 1% O₂ (72h). B) Following exposure to normoxia or hypoxia (72h), cells were re-plated (100 and 500 cells/well) and incubated during 11 days. Colonies were then fixed, stained, and the surviving fractions were calculated based upon the plating efficiency. C) Quantification of the average number of cristae in cells fixed *in situ* 96h following exposure to normoxia or hypoxia. Mean \pm SEM is representative of 2 independent experiments carried out in triplicate.

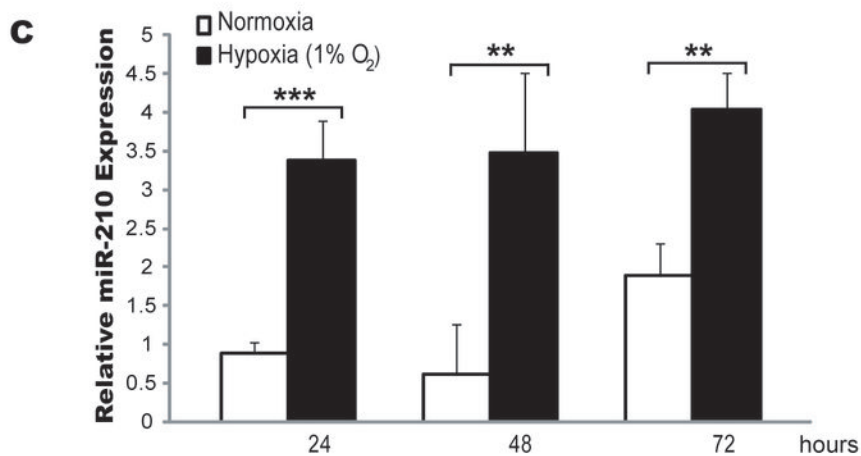
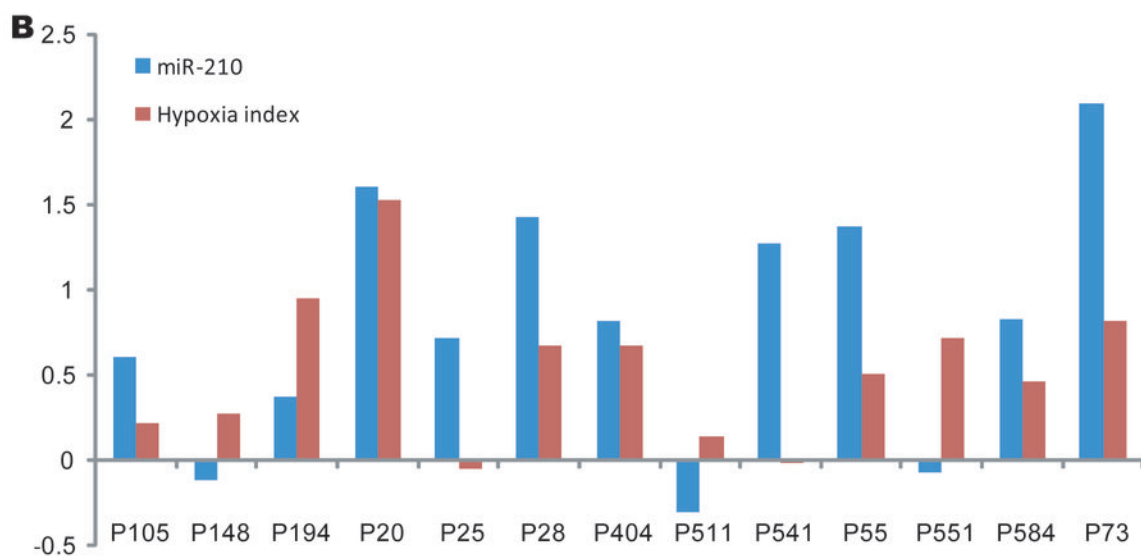
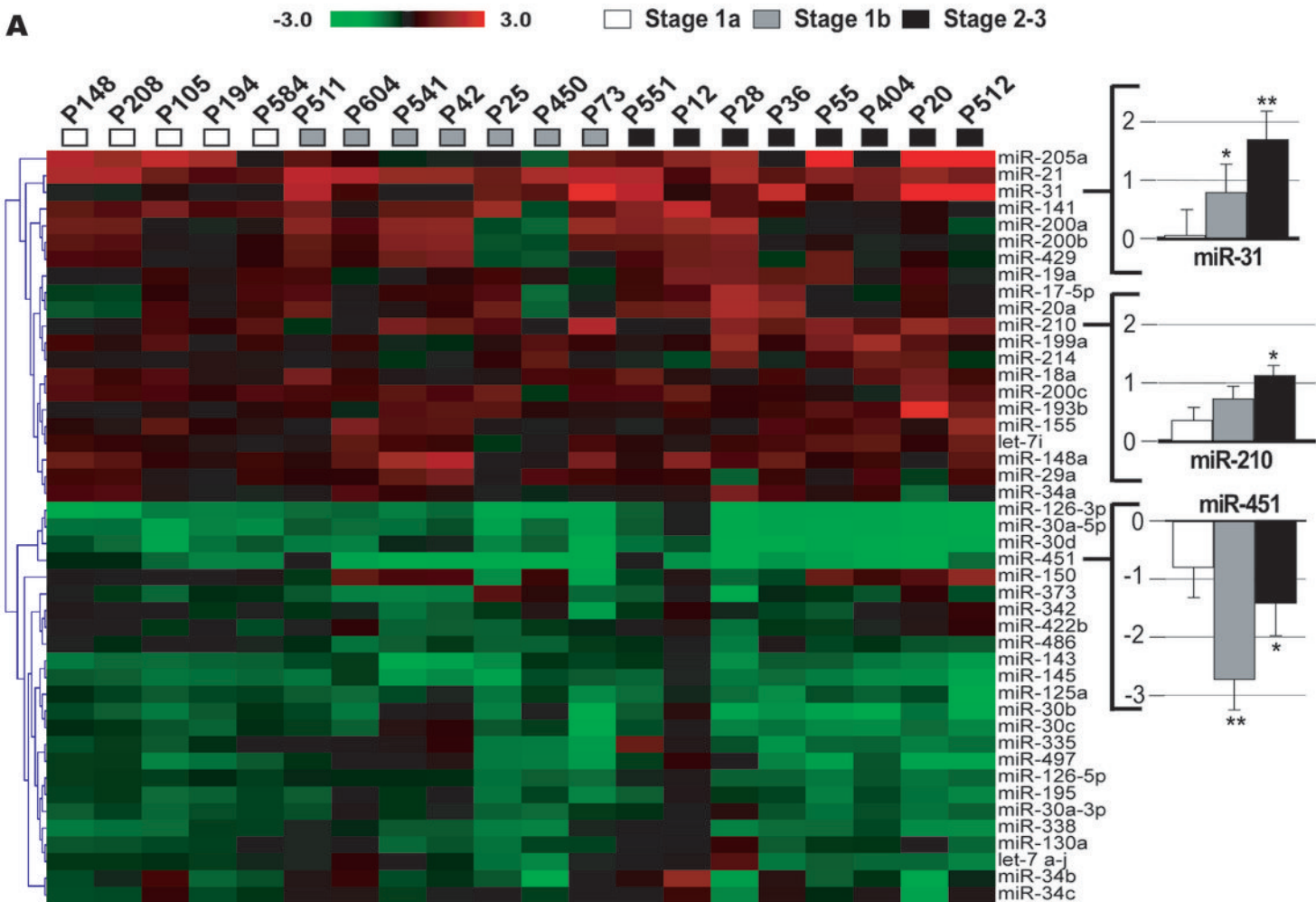
Figure 7. MiR-210 inhibition reduces HIF activity in hypoxic A549 cells. A549 cells were transfected with either pre-miR-Neg, pre-miR-210, a control anti-miR-159s LNA or anti-miR-210 in normoxia or hypoxia (1% O₂) and incubated for 48-72h. (A) Protein levels of HIF-1 α and of the loading control α -tubulin. (B) A549 cells were co-transfected with a HRE luciferase reporter and HIF activity was assessed using the dual luciferase reporter assay system 48h following transfection. Determinations were done in triplicate and the experiment was repeated three times. (C) The extracellular lactate concentration of transfected cells incubated in normoxia or hypoxia 1% O₂ for 48h was normalized to cell protein for each condition. Mean \pm SEM is representative of 3 independent experiments carried out in triplicate. (D) Proposed model for miR-210, SDHD and HIF-1 α inter-regulation. HIF-1 α up-regulates miR-210, which in turn

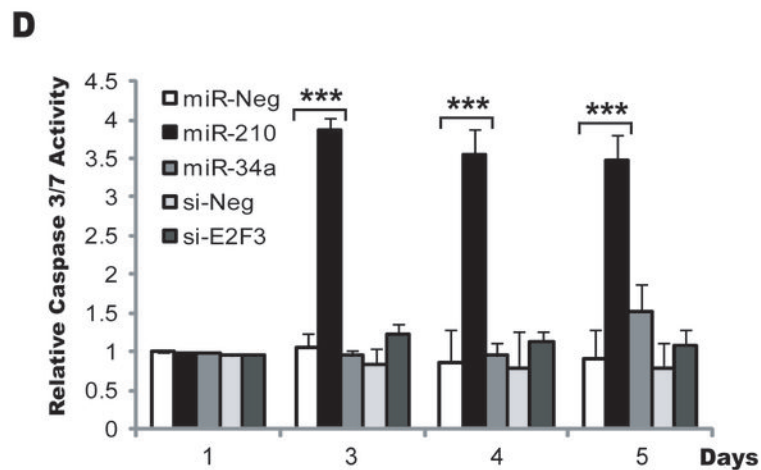
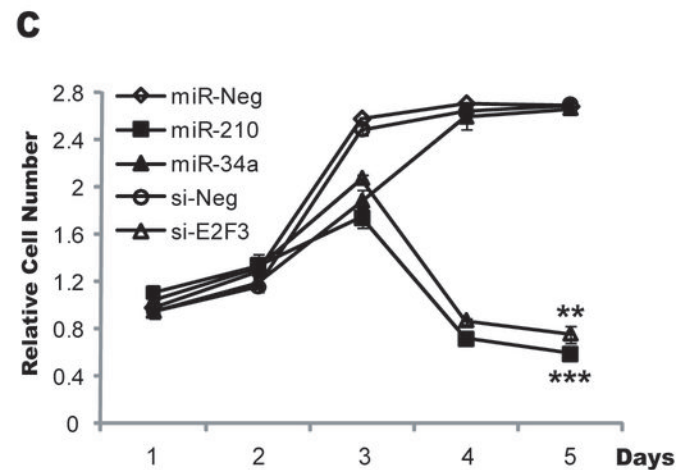
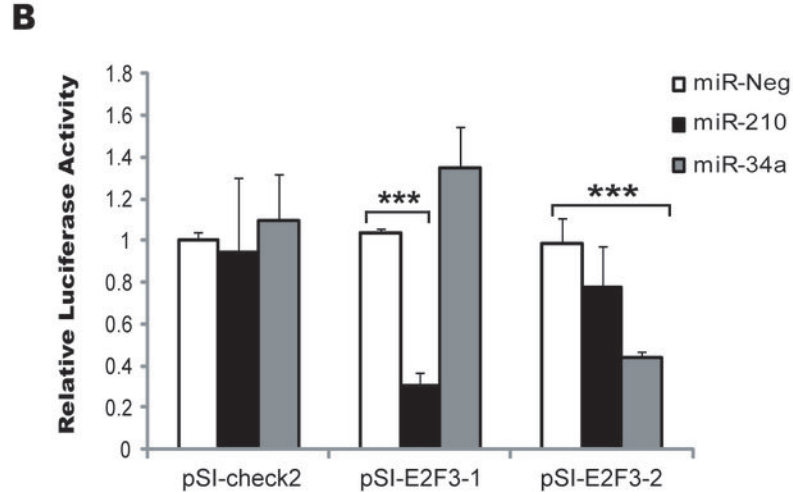
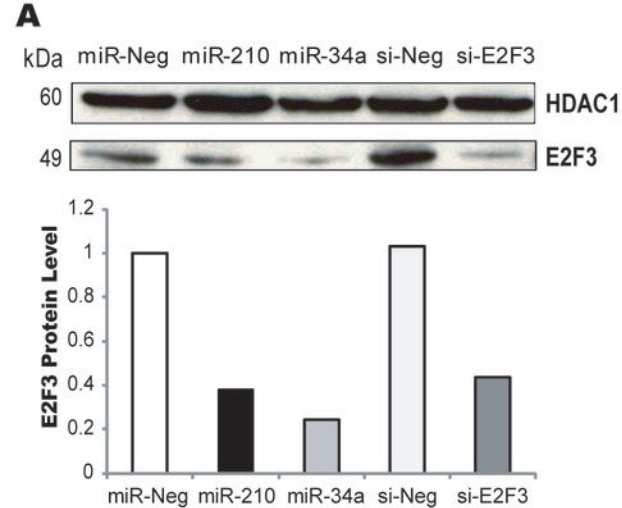
down-regulates SDHD, leading to complex II dysfunction. High succinate levels resulting from loss of complex II could inhibit the PHD activity giving HIF-1 α stabilization.

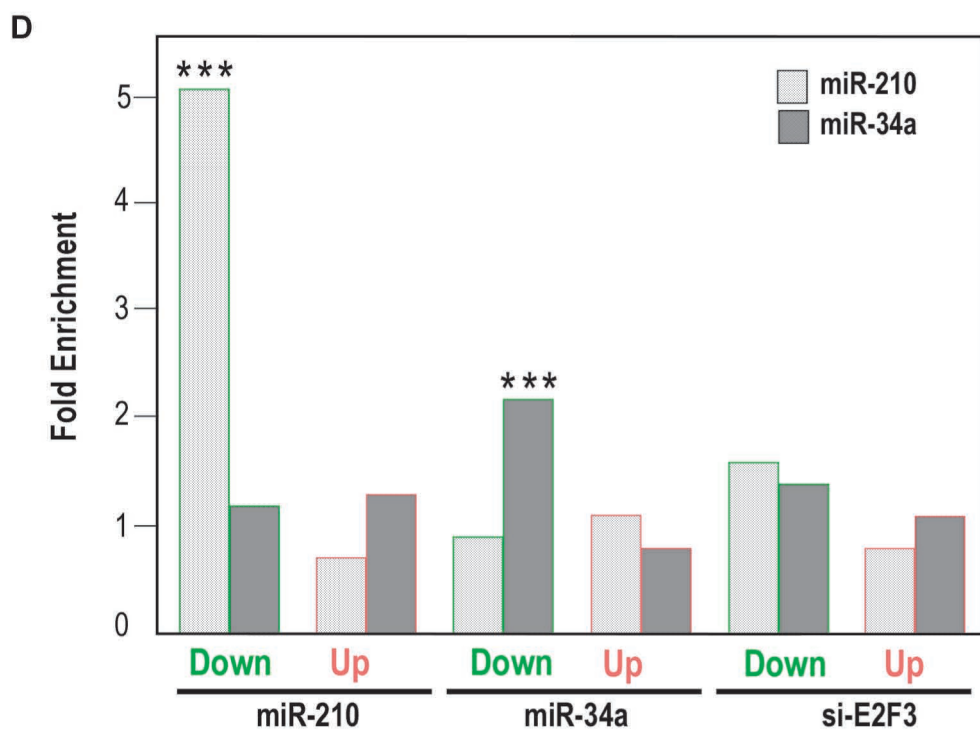
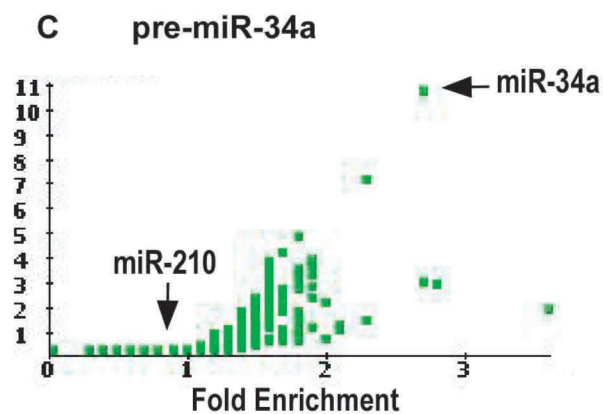
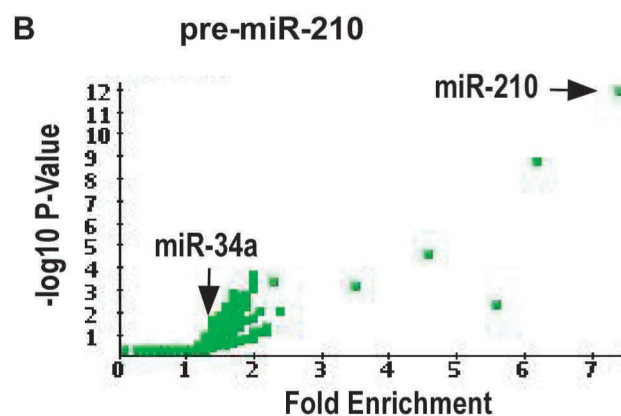
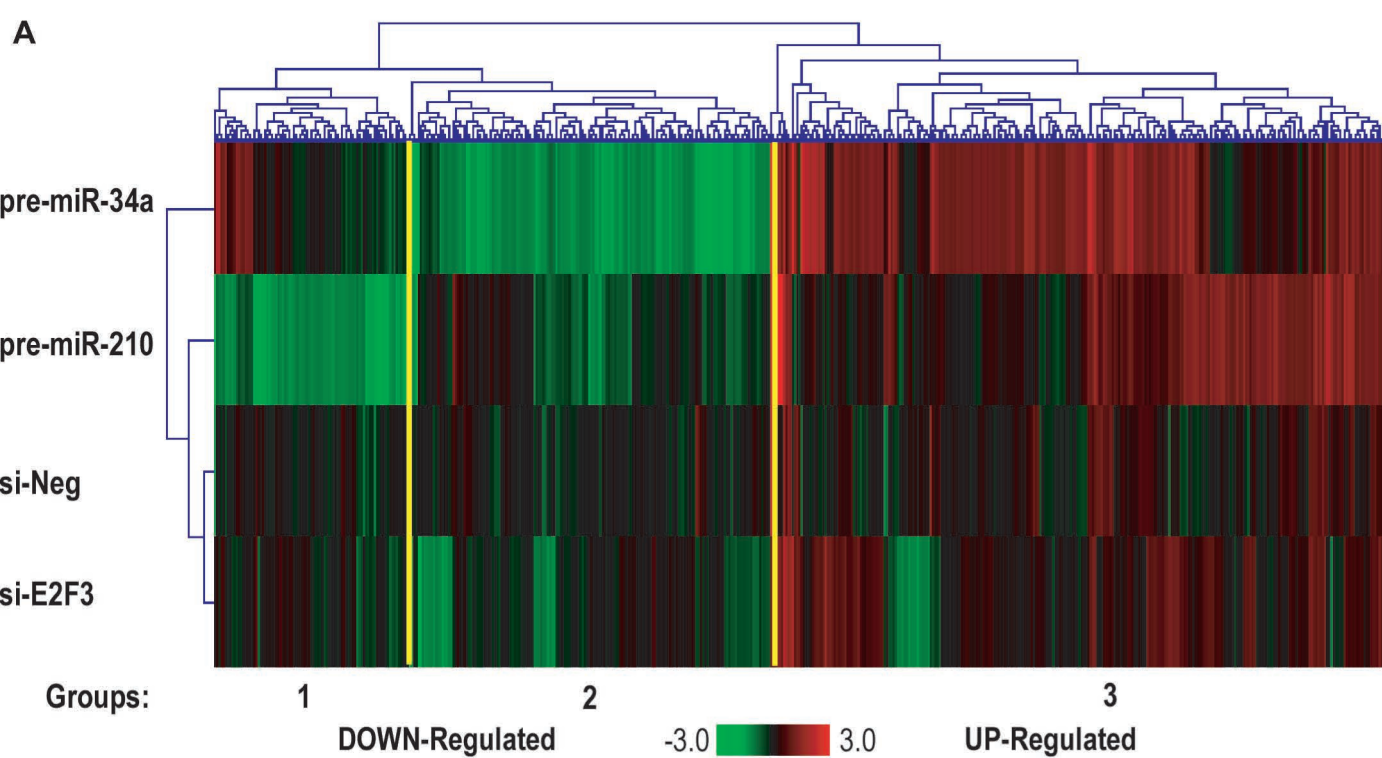
Symbol	ID	Genbank ID	Average Expr.	LogFC	accession_number	Description
ABCC3	102419	8714	13.2	-1.6	NM_020038	Homo sapiens ATP-binding cassette, sub-family C (CFTR/MRP), member 3 (ABCC3), transcript variant MRP3B, mRNA.
ABL1	10499	25	10.9	-1.3	NM_005157	Homo sapiens c-abl oncogene 1, receptor tyrosine kinase (ABL1), transcript variant a, mRNA.
ALDH5A1	63840	7915	9.3	-1.7	NM_170740	Homo sapiens aldehyde dehydrogenase 5 family, member A1 (ALDH5A1), nuclear gene encoding mitochondrial protein, transcript variant 1, mRNA.
C22orf9	120469	23313	9.2	-1.3	NM_015264	Homo sapiens chromosome 22 open reading frame 9 (C22orf9), transcript variant 1, mRNA.
CDCA7L	34411	55536	9.43	-1.13	NM_018719	Homo sapiens cell division cycle associated 7-like (CDCA7L), transcript variant 1, mRNA.
COL4A2	94674	1284	11.9	-2.5	NM_001846	Homo sapiens collagen, type IV, alpha 2 (COL4A2), mRNA.
DCBLD1	72084	285761	11.4	-1.6	AK055462	Homo sapiens cDNA FLJ30900 fis, clone FEBRA2005752.
DDOST	9043	1650	11.9	-1.6	NM_005216	Homo sapiens dolichyl-diphosphooligosaccharide-protein glycosyltransferase (DDOST), mRNA.
DHFR	90261	1719	12.4	-1.2	NM_000791	Homo sapiens dihydrofolate reductase (DHFR), mRNA.
DKFZp434H1419	77126	150967	8.8	-1.1	AL137534	Homo sapiens mRNA; cDNA DKFZp434H1419 (from clone DKFZp434H1419); partial cds.
EHD2	22648	30846	11	-1.4	NM_014601	Homo sapiens EH-domain containing 2 (EHD2), mRNA.
ELOF1	46850	84337	9.3	-1.2	NM_032377	Homo sapiens elongation factor 1 homolog (S. cerevisiae) (ELOF1), mRNA.
EPB41L1	174127	2036	10	-1.2	NM_012156	Homo sapiens erythrocyte membrane protein band 4.1-like 1 (EPB41L1), transcript variant 1, mRNA.
FAM102A	69086	399665	10.4	-1.3	NM_203305	Homo sapiens family with sequence similarity 102, member A (FAM102A), transcript variant 2, mRNA.
FAM3C	116003	10447	9.8	-1.1	NM_014888	Homo sapiens family with sequence similarity 3, member C (FAM3C), transcript variant 1, mRNA.
FKBP9	14807	11328	11.1	-1.1	NM_007270	Homo sapiens FK506 binding protein 9, 63 kDa (FKBP9), mRNA.
GDE1	31188	51573	9.37	-1.12	NM_016641	Homo sapiens glycerophosphodiester phosphodiesterase 1 (GDE1), mRNA.
GIT2	104909	9815	9.9	-1.6	NM_057169	Homo sapiens G protein-coupled receptor kinase interacting ArfGAP 2 (GIT2), transcript variant 1, mRNA.
H2AFY	167895	9555	12.4	-1.3	NM_001040158	Homo sapiens H2A histone family, member Y (H2AFY), transcript variant 4, mRNA.
HOXA1	11017	3198	9.6	-1.1	NM_005522	Homo sapiens homeobox A1 (HOXA1), transcript variant 1, mRNA.
INHBB	93581	3625	8.7	-1.4	NM_002193	Homo sapiens inhibin, beta B (INHBB), mRNA.
LASP1	14926	3927	13.3	-2.1	NM_006148	Homo sapiens LIM and SH3 protein 1 (LASP1), mRNA.
LHFP	9776	10186	9.7	-1.4	NM_005780	Homo sapiens lipoma HMGIC fusion partner (LHFP), mRNA.
MRPL36	48403	64979	12.3	-1.4	NM_032479	Homo sapiens mitochondrial ribosomal protein L36 (MRPL36), nuclear gene encoding mitochondrial protein, mRNA.
NDUFA4	93962	4697	14.8	-2.3	NM_002489	Homo sapiens NADH dehydrogenase (ubiquinone) 1 alpha subcomplex, 4, 9kDa (NDUFA4), nuclear gene encoding mitochondrial protein, mRNA.
NUP210	42162	23225	11.6	-1.3	NM_024923	Homo sapiens nucleoporin 210kDa (NUP210), mRNA.
PDXK	37342	8566	11	-1.5	NM_003681	Homo sapiens pyridoxal (pyridoxine, vitamin B6) kinase (PDXK), mRNA.
PSAP	132543	5660	11.7	-1.5	NM_002778	Homo sapiens prosaposin (PSAP), transcript variant 1, mRNA.
SCARA3	24194	51435	9.4	-1.9	NM_016240	Homo sapiens scavenger receptor class A, member 3 (SCARA3), transcript variant 1, mRNA.
SDF2	17519	6388	10	-1.4	NM_006923	Homo sapiens stromal cell-derived factor 2 (SDF2), mRNA.
SDHD	99293	6392	10.8	-1.4	NM_003002	Homo sapiens succinate dehydrogenase complex, subunit D, integral membrane protein (SDHD), nuclear gene encoding mitochondrial protein, mRNA.
SH3BGRL	97796	6451	11.1	-2	NM_003022	Homo sapiens SH3 domain binding glutamic acid-rich protein like (SH3BGRL), mRNA.
SIPA1L3	1390	23094	10	-1.4	NM_015073	Homo sapiens signal-induced proliferation-associated 1 like 3 (SIPA1L3), mRNA.
STAT6	97969	6778	10.6	-1.1	NM_003153	Homo sapiens signal transducer and activator of transcription 6, interleukin-4 induced (STAT6), mRNA.
TERF2IP	36068	54386	11.6	-1.4	NM_018975	Homo sapiens telomeric repeat binding factor 2, interacting protein (TERF2IP), mRNA.
TMEM80	79504	283232	11.5	-1.5	NM_001042463	Homo sapiens transmembrane protein 80 (TMEM80), transcript variant 2, mRNA.
TNPO3	18486	23534	10.5	-1.4	NM_012470	Homo sapiens transportin 3 (TNPO3), mRNA.
VAMP7	12699	6845	10.70	-1.66	NM_005638	Homo sapiens vesicle-associated membrane protein 7 (VAMP7), transcript variant 1, mRNA.

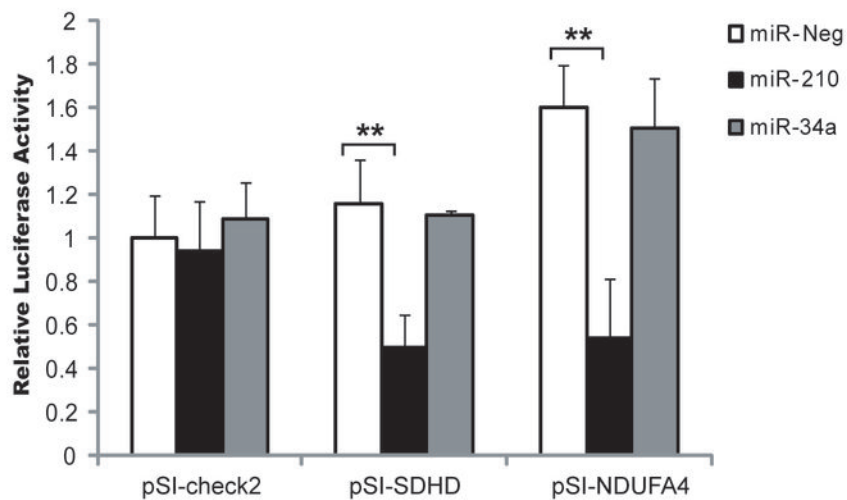
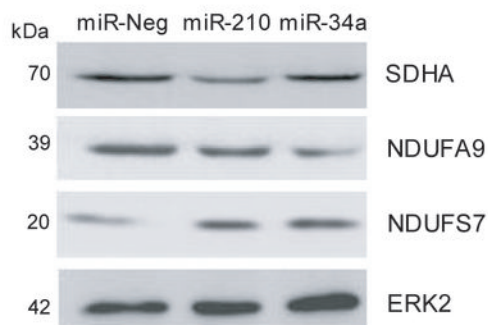
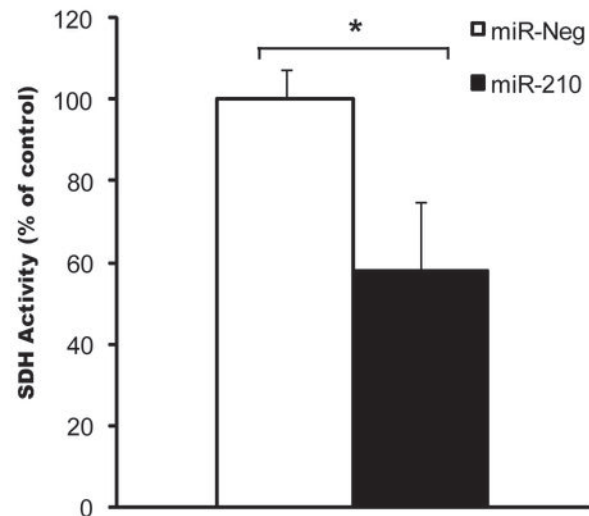
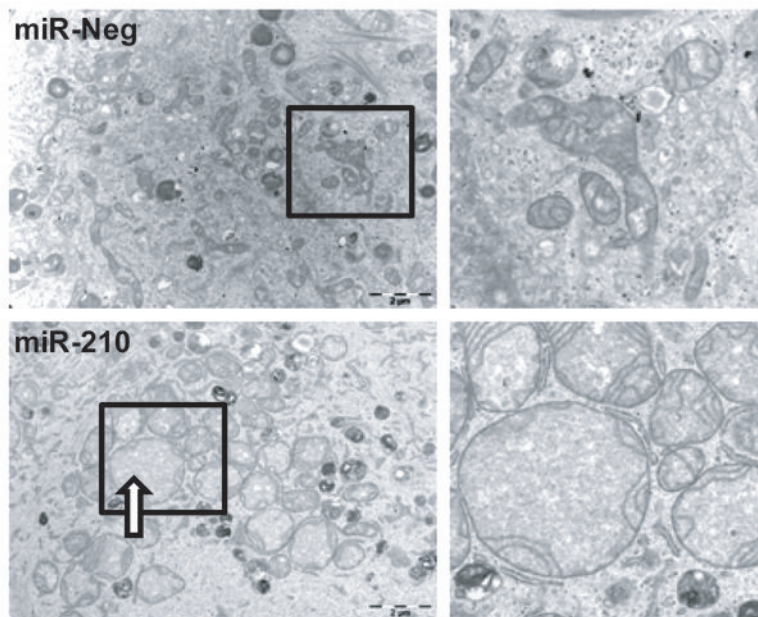
Table 1. List of the miR-210-predicted targets down-regulated following miR-210 overexpression in A549 cells.

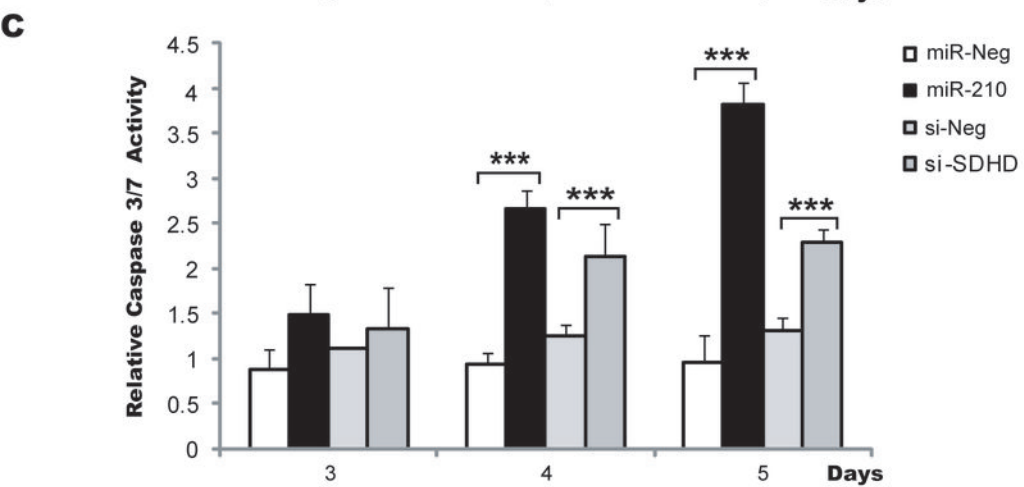
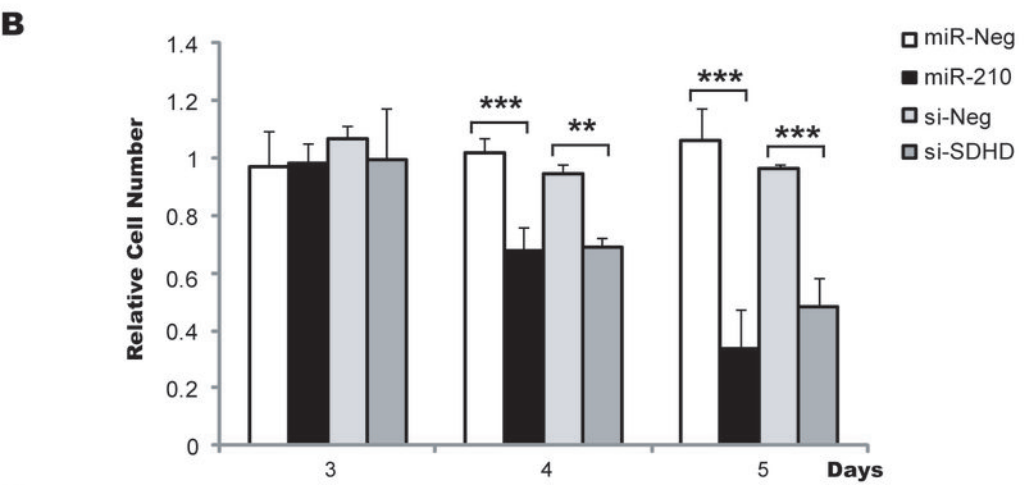
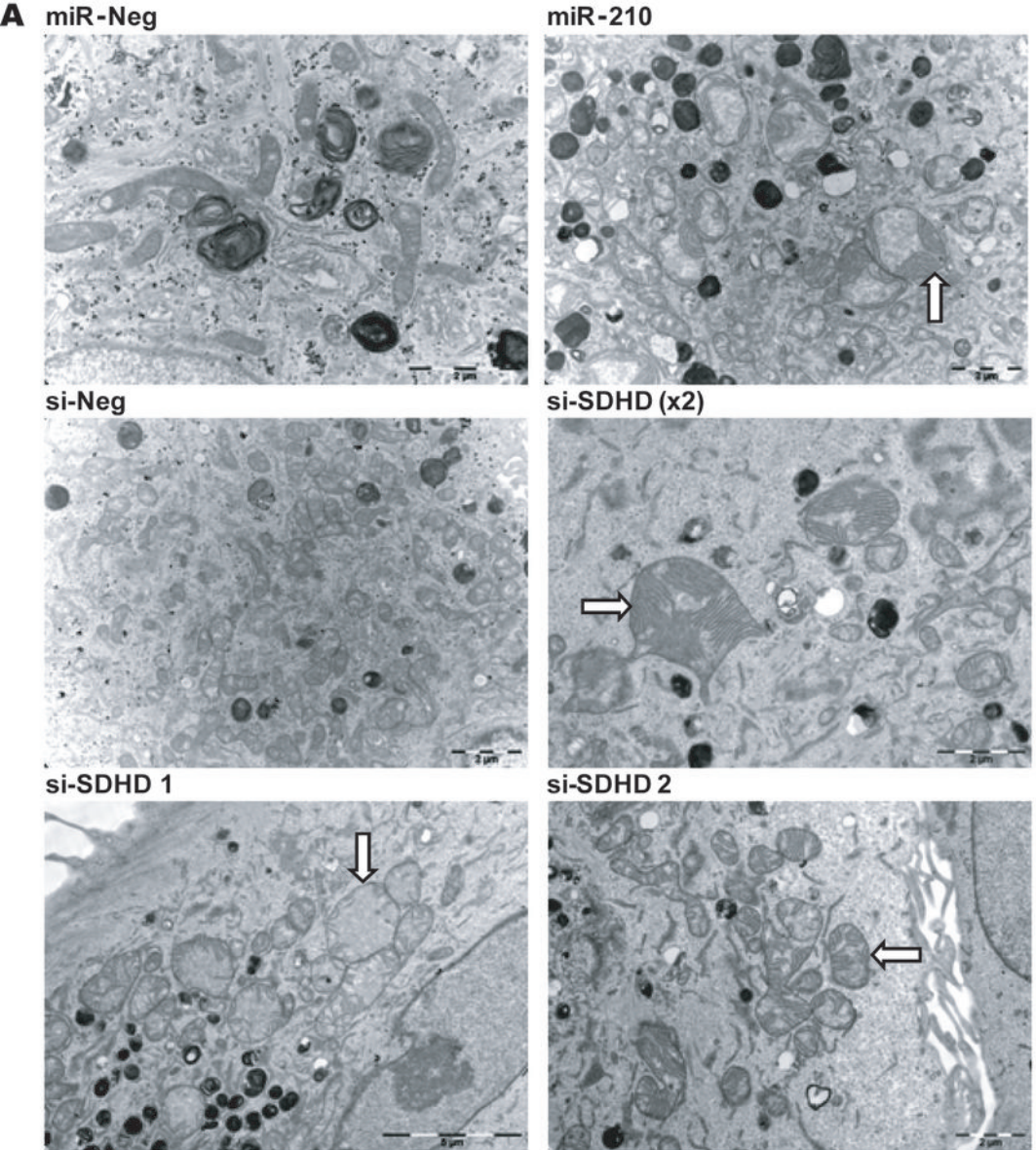
The 38 transcripts containing at least one complementary sequence to the “seed 2-7” of miR-210 in their 3’UTR and strongly repressed following miR-210 transfection are listed. Cut-offs for selection are equal to 8.0 for the \log_2 (signal), to -1 for the \log_2 (ratio), and to 0.001 for the adjusted p -value. Logarithm (base 2) of the ratio of miR-210 / miR-Neg is represented. ID: corresponds to RNG oligo IDs that gives access to transcripts and probes annotations through our information system Mediante (<http://www.microarray.fr:8080/merge/index>).

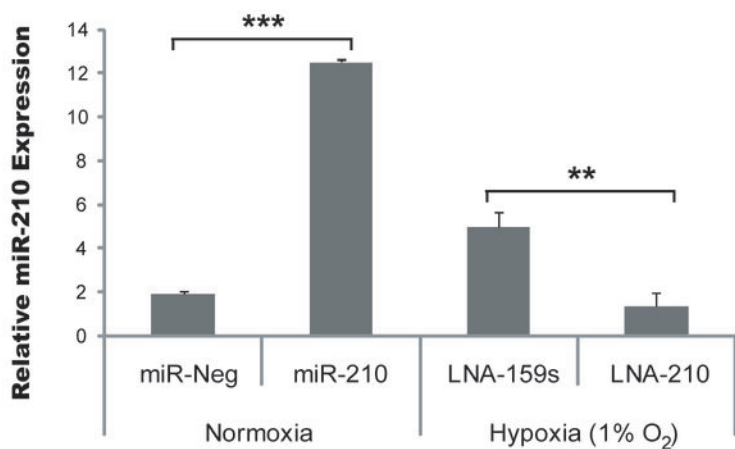
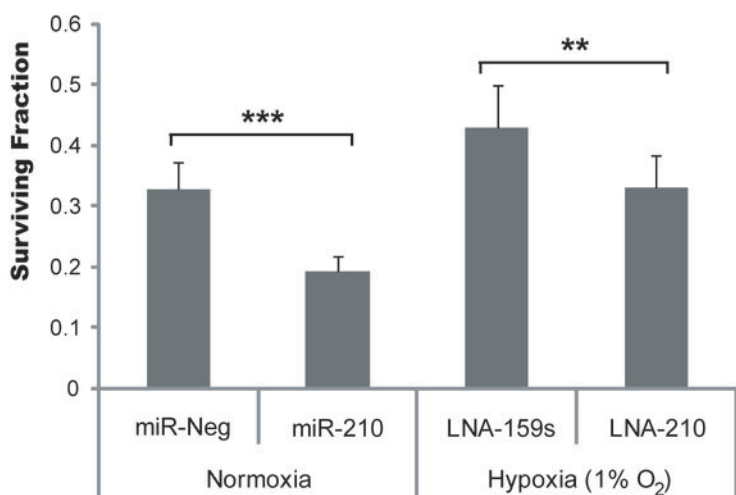
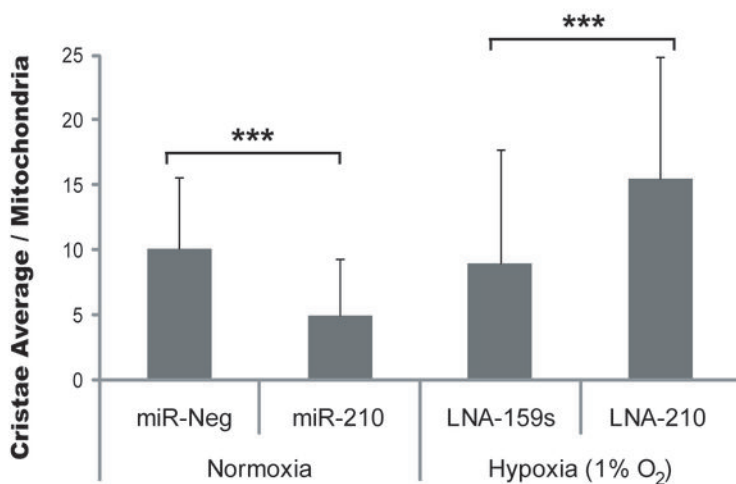


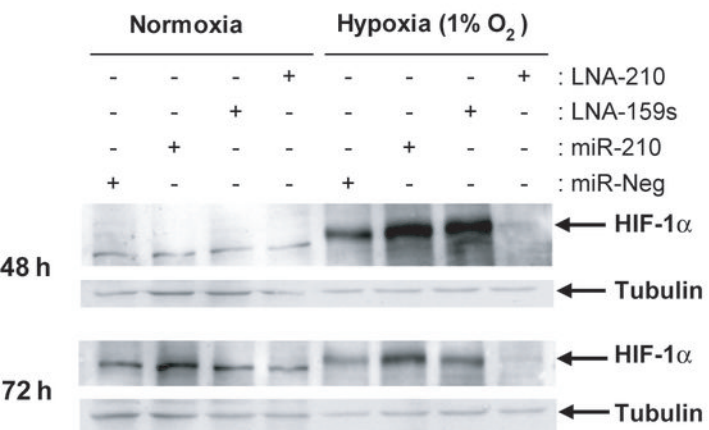
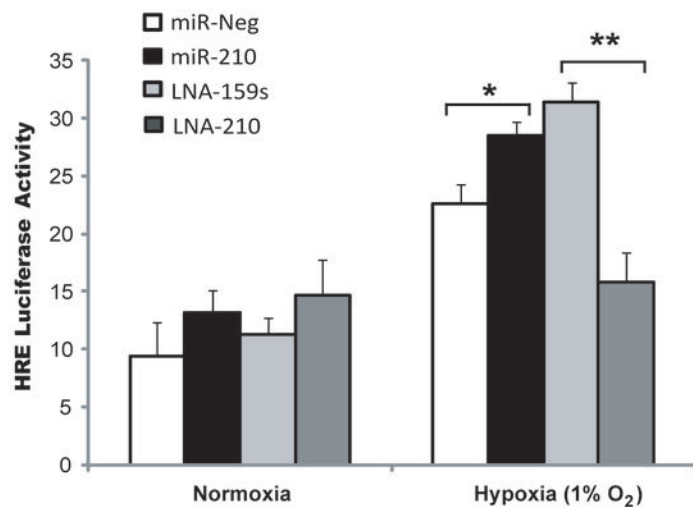
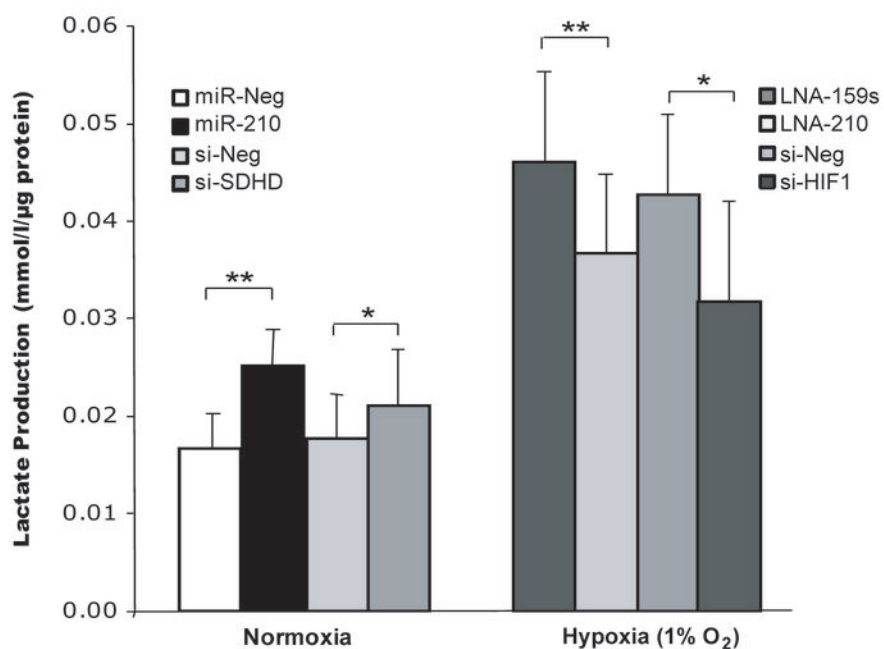




A**B****C****D**



A**B****C**

A**B****C****D**